

POLITECNICO DI TORINO

Master of Science in Mechanical Engineering



Master Thesis

**DILUTED COMBUSTION CHARACTERIZATION IN A DIRECT
INJECTION NG ENGINE BY MEANS OF CFD SIMULATION**

Supervisor:

Mirko BARATTA

Daniela MISUL

Ezio SPESSA

Candidate:

Teresa VARIALE

April 2018

*"There's no lemon so sour
that you can't make something
resembling lemonade"*

Contents

List of Figures	4
List of Tables	7
1 Introduction	9
1.1 Advantages of Natural Gas	11
2 Computational Fluid Dynamics	13
2.1 Introduction	13
2.2 Finite Volume Method	14
2.3 Navier-Stokes Equations	17
2.3.1 Continuity Equation	17
2.3.2 Momentum Equation	18
2.3.3 Energy Equation	19
2.4 Turbulent Flows	19
2.4.1 Direct Numerical Simulation (DNS)	20
2.4.2 Large Eddy Simulation (LES)	20
2.4.3 RANS Equations	20
2.5 Grid Generation and Control	22
2.5.1 Grid Scaling	23
2.5.2 Fixed Embedding	23
2.5.3 Adaptive Mesh Refinement (AMR)	25

3	Turbulent Combustion	27
3.1	Laminar and Turbulent Burning Velocities	28
3.1.1	Correlation in ICE	29
3.1.2	Turbulent Flame Speed	30
3.2	Regimes for Premixed Turbulent Combustion	31
3.2.1	Differences between Regimes	33
3.3	Extended Coherent Flame Model	34
3.3.1	Flamelet assumption	36
4	CFD Model set-up and Simulations	37
4.1	Simulation settings	37
4.1.1	Grid settings	38
4.1.2	Physical models	39
4.1.3	Numerical settings	41
4.2	Model Validation	42
4.2.1	2000x30 NOEGR case	42
5	EGR Sweep	49
5.1	EGR Sweep strategy	49
5.2	3D Data Analysis	62
5.2.1	yCH ₄	63
5.2.2	Temperature	69
5.2.3	Tumble	80
6	Conclusion	84
	Bibliography	85

List of Figures

1.1	2020 emissions targets	10
1.2	GasOn Project structure	11
2.1	Finite Volume Method	14
2.2	Solution order of the transport equation	16
2.3	Example of Fixed Embedding	24
3.1	Flame Front regions	28
3.2	Correlation for s_L	30
3.3	Borghi Plot	32
3.4	Scheme of ECFM model	35
3.5	Definition of flamlet assumption	36
4.1	3D Model	38
4.2	Scheme of inductive system	40
4.3	In-cylinder pressure - 2000x30 NOEGR	42
4.4	Average pressure cycle - 2000x30 NOEGR	43
4.5	Average heat release - 2000x30 NOEGR	43
4.6	Combustion detail, cycle 2 - 2000x30 NOEGR	44
4.7	Combustion detail, cycle 3 - 2000x30 NOEGR	44
4.8	Combustion detail, cycle 4 - 2000x30 NOEGR	45
4.9	Combustion detail, cycle 5 - 2000x30 NOEGR	45

4.10	Combustion detail, cycle 6 - 2000x30 NOEGR	46
4.11	Combustion detail, cycle 7 - 2000x30 NOEGR	46
4.12	Combustion detail, cycle 8 - 2000x30 NOEGR	47
4.13	Average pressure cycle - Comparison	48
4.14	Average Heat Release cycle - Comparison	48
5.1	EGR Sweep strategy	49
5.2	CoV imep for different EGR rates - 2000x8	51
5.3	CoV imep for different EGR rates - 3000x8	51
5.4	CoV imep for different EGR rates - 2000x30	52
5.5	CoV imep vs MFB0-50 - 2000x8	52
5.6	CoV imep vs MFB0-50 - 3000x8	53
5.7	CoV imep vs MFB0-50 - 2000x30	53
5.8	Average pressure cycle comparison - 2000x8	54
5.9	Average heat release comparison - 2000x8	55
5.10	Average pressure cycle comparison - 2000x30	55
5.11	Average heat release comparison - 2000x30	56
5.12	Tumble for different EGR rates - 2000x8	56
5.13	Tumble for different EGR rates - 2000x30	57
5.14	Tumble for different EGR rates - 3000x8	57
5.15	Turbulent intensity for different EGR rates - 2000x8	57
5.16	Turbulent intensity for different EGR rates - 2000x30	58
5.17	Turbulent intensity for different EGR rates - 3000x8	58
5.18	Ensamble average of Tumble - 2000x8	59
5.19	Ensamble average of Tumble - 2000x30	59
5.20	Ensamble average of Tumble - 3000x8	60
5.21	Ensamble average of turbulent intensity - 2000x8	60
5.22	Ensamble average of turbulent intensity - 2000x30	61
5.23	Ensamble average of turbulent intensity - 3000x8	61

5.24	CH4 at 10 degCA after spark - 2000x8	63
5.25	CH4 at 20 degCA after spark - 2000x8	64
5.26	CH4 at 30 degCA after spark - 2000x8	64
5.27	CH4 at 40 degCA after spark - 2000x8	65
5.28	CH4 at 10 degCA after spark - 2000x30	66
5.29	CH4 at 20 degCA after spark - 2000x30	67
5.30	CH4 at 40 degCA after spark - 2000x30	68
5.31	Temperature at 5 degCA before spark- 2000x8	69
5.32	Temperature at spark advance- 2000x8	70
5.33	Temperature at 5 degCA before spark- 2000x8	70
5.34	Temperature at 840 degCA - 2000x8	71
5.35	Temperature at 885 degCA - 2000x8	71
5.36	Temperature at 900 degCA - 2000x8	72
5.37	Temperature at 930 degCA - 2000x8	72
5.38	Temperature at 960 degCA - 2000x8	73
5.39	Temperature at 5 degCA before spark - 2000x30	74
5.40	Temperature at spark advance - 2000x30	75
5.41	Temperature at 5 degCA after spark - 2000x30	76
5.42	Temperature at 885 degCA - 2000x30	77
5.43	Temperature at 900 degCA - 2000x30	78
5.44	Temperature at 810 degCA - 2000x30	79
5.45	Temperature at 960 degCA - 2000x30	80
5.46	Tumble at 180 degCA before spark	81
5.47	Tumble at 150 degCA before spark	81
5.48	Tumble at 80 degCA before spark	82
5.49	Tumble at 50 degCA before spark	82
5.50	Tumble at 20 degCA before spark	83
5.51	Tumble at spark advance	83

List of Tables

4.1	Adaptive mash refinement	38
4.2	Fixed Embedding	39
4.3	Numerical settings	41
5.1	List of all cases	50

Abstract

In recent years, a great increment in CO₂ emission, has been recorded, with serious consequence both for environment and human health. Internal Combustion Engine (ICE) with its emission, is one of the responsible of this pollution, hence improvements in powertrain and alternative fuel with a minor contents of carbon are needed. In this context GasOn project takes place. Its first aim is to reducing the CO₂ emissions by the 20% in 2020, developing a CNG-only, mono-fuel engine. The project is divided in sub-projects, each of them refers to a different technology: Variable Valve Actuator, variable compression ratio, combustion. In particular this work belongs to the WP4 part of the project which deals with charge dilution and exhaust gas temperature control.

The work has been developed in Energy department of Politecnico di Torino, in a research team managed by the professor M. Baratta, D. Misul, E. Spessa. 3D-CFD simulations has been carried out, based on the engine model. The beginning of the work describes computational fluid dynamics technique, governing equations, turbulent combustion characteristics and models used. Then is presented the experimental work. The first part deals with the calibration of the model through experimental data provided by partners. Once calibrated, the model is used as predictive, for simulations of points not covered by experiments, both with and without EGR. Diluted combustion characterization occupy the greater part of the thesis, and how combustion and performance vary changing EGR rate is studied.

Chapter 1

Introduction

In the recent years the percentage of carbon dioxide, CO_2 , in the atmosphere has reached the highest level of the last decade. As a greenhouse gas, its excess dramatically influence both environment and human health. Greenhouse gas are normally present in the atmosphere and they allow the sunlight radiation to pass freely through atmosphere and hit the earth surface. Some of these radiations are absorbed by earth, the remaining part is delivered as heat. Some of this is intercepted and absorbed by greenhouse gases, enhancing the global temperature. Thus the first environmental effect is climate change, earth's surface has strongly increased as well as oceans' level. Human health is effected by these gases too, in particular by CO_2 , since it replace oxygen and make breathing more difficult, with serious consequences for men.

Greenhouse gas include also Nitrous Oxide, Methane, but the major part is represented by Carbon Dioxide [1]. Mankind has the responsibility of its excessive presence firstly owing to deforestation, which subtract plants from the planet that have the important role to absorb carbon dioxide from air. However the larger source comes from combustion of fossil fuels in industry, energy sector and transports. Nowadays, in automotive field, there are regulations which set the limits for exhaust emissions. In particular for CO_2 the current standard is EC 443/2009

which regulates the average specific emissions for new passenger vehicles and defines penalties for manufacturers in case of surplus. Starting from 2020, more restrictive limits will come into force, as described in the following figure [2]:

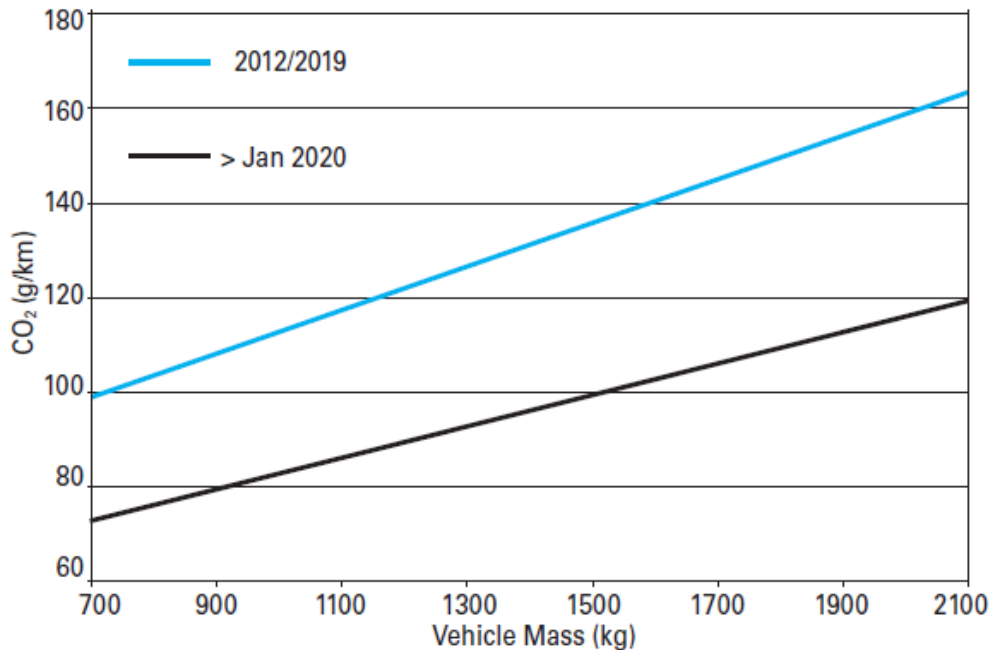


Figure 1.1. 2020 emissions targets

Since in 2030 more than 65% of all road transport vehicles will be still powered by Internal Combustion Engines (ICE) [3], improvement in powertrain for enhancing energy efficiency and investigation of alternative fuels are needed in order to respect the new standard. Along with CO₂ emissions reduction, the choice of low carbon alternative fuels turn out to be convenient also for the drop of air pollution due to transportation vehicles (i.e. NO_x, CO, particular matter). This road will bring benefits also from a security and economics point of view: these new fuels will decrease progressively the dependence on crude oil and will be cheaper than the traditional gasoline and diesel.

In this scenario, the European GasOn project takes place. Its aim is to develop

a CNG-only, mono-fuel engine in order to deal with new regulations, new homologation cycle and real driving conditions and to improve engine efficiency and vehicle performance also with regard to its CNG range capability. New technologies for both advanced combustion and innovative injection system are examined. The simultaneous improvement of air, combustion, ignition and injection management can provide huge benefits, in comparison with previous approaches adopting single technology [3]. The structure of the project is presented in the diagram below.

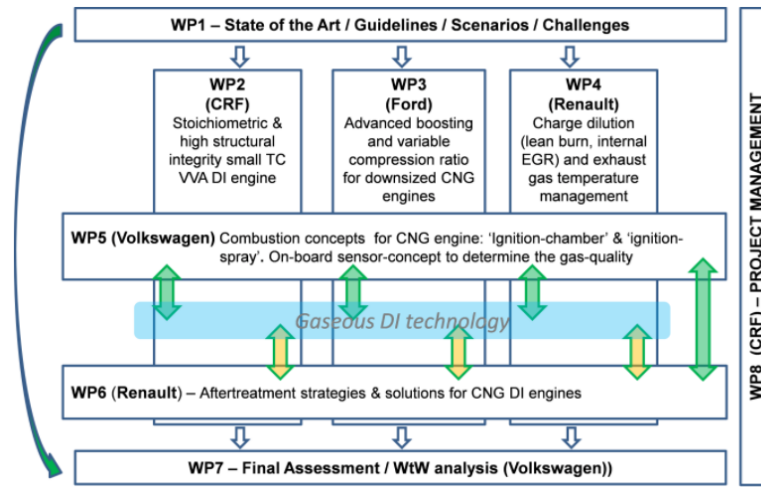


Figure 1.2. GasOn Project structure [3]

In particular, this work belongs to WP4 section, which deals with charge dilution and exhaust gas temperature control, and involves Renault, IFP, Continental and Politecnico di Torino.

1.1 Advantages of Natural Gas

Natural Gas is a fossil fuel whose primary constituent is methane. As energy vector, it has the great quality to allow energy diversification and, by consequence, decrease the dependence on cruel oil, since it has large stocks. Natural gas' combustion is the cleanest compared to other fossil fuel. For this reason, only few

pollutants are emitted in the atmosphere at the end of the process and it doesn't leave behind any soot and ash.

In automotive field, particular properties make natural gas attractive for internal combustion engine working. These have been investigated in several paper in which performance and emissions of CNG engine are compared to those of gasoline and diesel engine.

Natural gas has the great characteristic to have a high knock resistance due to its octane number (approximately 130) which allows higher compression ratio operation and accordingly a higher thermal efficiency. Moreover its low carbon-to-hydrogen ratio leads to lower CO₂ exhaust emissions, as discussed above [4]. T. Korakianitis et al. studied performance and emission of natural gas fuelled spark ignition (SI) and compression ignition (CI) engine. The results certify that since these engine use high compression ratio and advanced spark time, NO_x increase; on the other hand a reduction in CO and overall HC is reported. EGR could play an important role for emissions, in fact the recirculation of exhaust gas lower temperature and oxygen contents, abating NO_x but increasing HC and CO. Thus to obtain the maximum benefit from both engine, some optimizations are required. SI engine operating at high load can work with high EGR rates, while advanced spark time and high compression ratio enhance power output [5].

A strategy to improve natural gas SI engine, is direct injection. It is proved that replacing gasoline with NG in port injection results in a reduction in power, volume efficiency and BMEP [6]. Directly injecting fuel in combustion chamber allow to get over it whereas it enhance turbulent intensity, improving mixing process and increasing combustion efficiency. Still it will be a smoke free operation typical of SI engine and lower NO_x emissions compared to diesel engine are recorded.

Chapter 2

Computational Fluid Dynamics

2.1 Introduction

Computational fluid dynamics (CFD) is a branch of fluid mechanics that allows the simulation of real flows by the numerical solution of the governing equations of the problem i.e. continuity, momentum and the energy equation [7]. The most efficient mean for knowing global parameters in a problem has always been experiment. Having the right tool and following the right procedure allow you to achieve great results with an acceptable accuracy. However experiment settings could be expensive both in terms of time and money and all physical information could be available. An alternative method is needed and CFD, in the last years, has confirmed its applicability in partially replacing experimental tasks.

The aim of this technique is to replace the partial differential (or integral-differential) equations which cannot be always solve analytically, with a system of algebric equations in order to understand how the flow behave in a particular system with particular boundary conditions. Original equations have to be approximated by a discretization method. The approximations are applied to small domains in space and time and the accuracy of the solution depends on the kind of method used. If you want more rigorous results, it's better to discretize the

equations in smaller domain, enhancing not only the accuracy, but also the time and the cost required. Several numerical methods were developed more than a century ago. However it was difficult to apply them without a support, represented by computers. Their continuous improvement in speed, ability to store data and performance to cost ratio, has helped the spread of computational techniques; as a result the study of fluid flows has become easier and more effective [10].

2.2 Finite Volume Method

The discrete locations at which the variables are to be calculated are defined by a numerical grid which is the representation of the geometric domain on which the problem is to be solved [10].

The Finite Volume Method (FVM) is one of the most versatile discretization techniques used in CFD since it can accommodate any type of grid, so it is suitable for complex geometry. The first step is to divide the domain into a number of control volumes and the conservation equations are applied in each centroid: in these computational nodes the variable of interest have to be calculated.

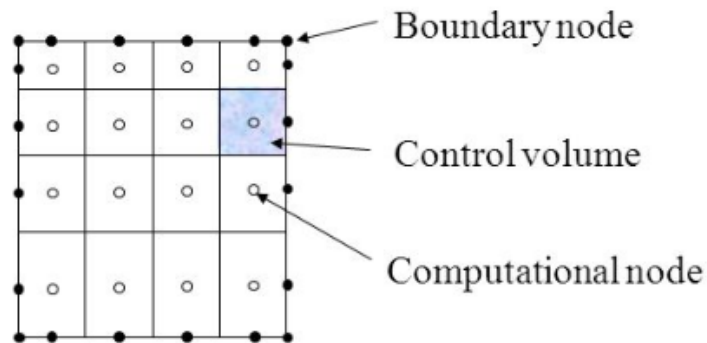


Figure 2.1. Finite Volume Method

Now consider the simple transport equation:

$$\frac{\partial \phi}{\partial t} + \frac{\partial u \phi}{\partial x} = 0 \quad (2.1)$$

The above equation can be written in integral form as:

$$\frac{d}{dt} \int_V \phi dV + \int_S u * n \phi dS = 0 \quad (2.2)$$

where V is the cell volume, S is the surface area, and n is the surface normal. The integral form of the equation is solved by summing fluxes on the faces of the cells and all the values are collocated and stored at the center of the cell. Every volume borders with the others, thus fluxes through the boundaries are related to the centroids of adjacent volume. One option is to average the two adjacent cell values and place them on the surface:

$$\phi_{i+1/2} = \frac{1}{2}\phi_i + \frac{1}{2}\phi_{i+1} \quad (2.3)$$

$$\phi_{i-1/2} = \frac{1}{2}\phi_i + \frac{1}{2}\phi_{i-1} \quad (2.4)$$

Another option is to upwind the surface value as follows:

$$\phi_{i+\frac{1}{2}} = \phi_i \quad (2.5)$$

$$\phi_{i-\frac{1}{2}} = \phi_{i-1} \quad (2.6)$$

The results of the discretization process is a system of algebraic equations, which are linear or non-linear according to the nature of the partial differential equations from which they are derived. Usually they are solved with iterative technique that involves guessing a solution, linearizing the equations about that solution, and improving the solution. In CONVERGE, the software used in this work, the solving steps are listed in Figure 2.2.

At the beginning, the previous values are stored for all transport quantities. Then sources for each sub-models are calculated and radiation is solved if it's decoupled with energy. From this moment, PISO loop begins. PISO stands for Pressure Implicit with Splitting of Operators (Issa (1986), [8]) and its first step is to predict a value in order to solve momentum equation.

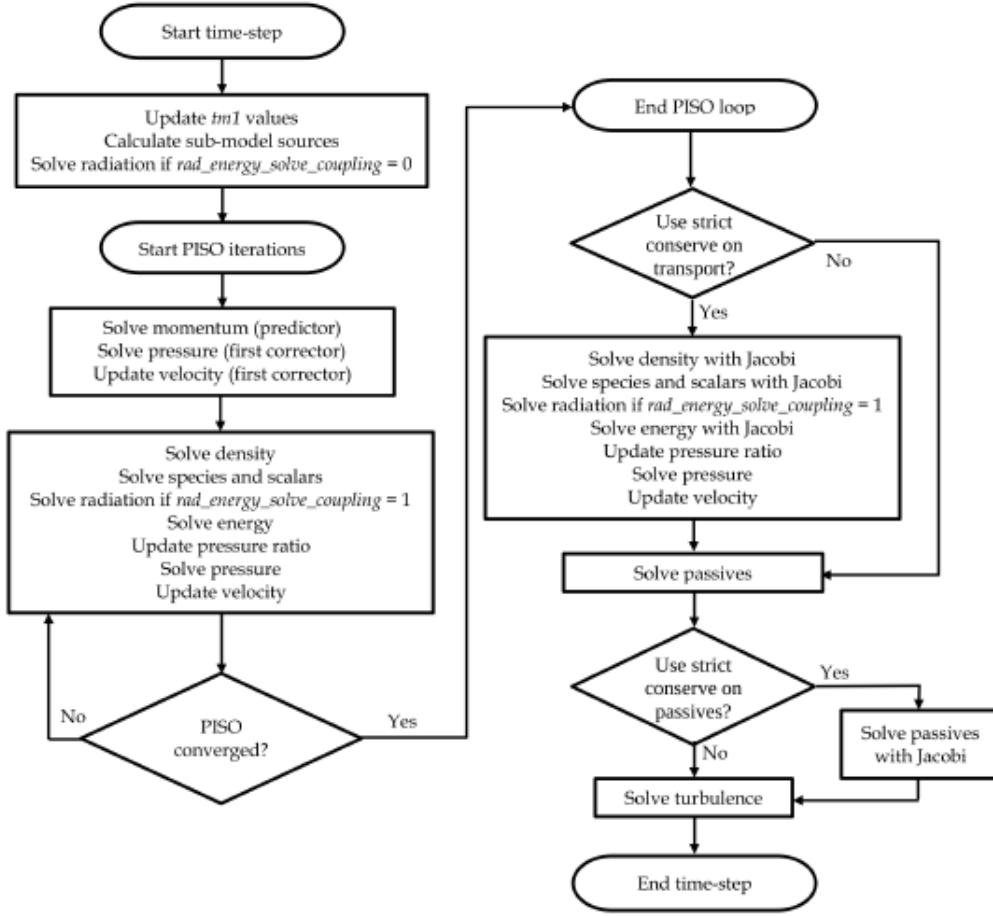


Figure 2.2. Solution order of the transport equation [8]

After the predictor step, pressure equations is solved, correcting the momentum equation and, by consequence, obtaining the velocity value which is needed to solve the other transport equations in series. After that, PISO convergence is checked: if it converge, then PISO loop ends, in the other case, transport equations have to be recalculated.

The momentum equations has to be corrected and resolved until the desired accuracy is achieved and thus until the tolerance reaches the desired value [8]:

$$\frac{|\psi_i^{**} - \psi_i^*|}{|\psi_i^{**}|} < tol \quad (2.7)$$

User can set the maximum and minimum number of correction: if this limits are not respected, the time step will be changed.

2.3 Navier-Stokes Equations

The dynamics of fluid flow are governed by equations that describe the conservation of mass, momentum, and energy which represent the interrelationship between the flow variables and their evolution in time and space.

Consider a general flow field and imagine a closed volume drawn within a finite region of the flow. This volume defines a control volume, V , and a control surface, S , is defined as the closed surface which bounds the volume. The control volume may be fixed in space with the fluid moving through it. The fundamental physical principles are applied to the fluid inside the control volume and to the fluid crossing the control surface [9]. The fluid flow equations that we directly obtain by applying the fundamental physical principles to a finite control volume are in integral form. These integral forms of the governing equations can be manipulated to indirectly obtain partial differential equations.

2.3.1 Continuity Equation

The rate of decrease of mass inside the control volume V , must equal the total rate of mass flux out of V :

$$-\int_V \frac{\partial \rho}{\partial t} dt = \int_S \rho \vec{v} dS = \int_V \nabla \cdot (\rho \vec{v}) dV \quad (2.8)$$

In the partial differential form:

$$\frac{\partial \rho}{\partial t} + \frac{\partial(\rho u)}{\partial x} + \frac{\partial(\rho v)}{\partial y} + \frac{\partial(\rho w)}{\partial z} = 0 \quad (2.9)$$

2.3.2 Momentum Equation

The rate of change of momentum must equal the net force on the element. Actually there are two different types of forces that act in any fluid:

- External body forces that penetrate matter and act equally on all the material in any element dV (i.e. gravity), contained in the term F ;
- Molecular forces, internal to the fluid and due to interactions with other elements. This kind of forces are expressed by the stress tensor, T . Any element is a combination of pressure e viscous friction and could be described by a constitutive relation. For Newtonian, isotropic fluid and incompressible flow:

$$T_{ij} = -p\delta_{ij} + \mu\left(\frac{\partial u_i}{\partial x_j} + \frac{\partial u_j}{\partial x_i}\right) \quad (2.10)$$

According to these considerations, the resulting conservation equation for each component x, y, z , is:

$$\rho\left(\frac{\partial u}{\partial t} + u\frac{\partial u}{\partial x} + v\frac{\partial u}{\partial y} + w\frac{\partial u}{\partial z}\right) = -\frac{\partial p}{\partial x} + \mu\left(\frac{\partial^2 u}{\partial x^2} + \frac{\partial^2 u}{\partial y^2} + \frac{\partial^2 u}{\partial z^2}\right) + F_x \quad (2.11)$$

$$\rho\left(\frac{\partial v}{\partial t} + u\frac{\partial v}{\partial x} + v\frac{\partial v}{\partial y} + w\frac{\partial v}{\partial z}\right) = -\frac{\partial p}{\partial y} + \mu\left(\frac{\partial^2 v}{\partial x^2} + \frac{\partial^2 v}{\partial y^2} + \frac{\partial^2 v}{\partial z^2}\right) + F_y \quad (2.12)$$

$$\rho\left(\frac{\partial w}{\partial t} + u\frac{\partial w}{\partial x} + v\frac{\partial w}{\partial y} + w\frac{\partial w}{\partial z}\right) = -\frac{\partial p}{\partial z} + \mu\left(\frac{\partial^2 w}{\partial x^2} + \frac{\partial^2 w}{\partial y^2} + \frac{\partial^2 w}{\partial z^2}\right) + F_z \quad (2.13)$$

The terms on the left hand side are often referred to as inertial terms, and arise from the momentum changes. These are countered by the pressure gradient, viscous forces which always act to retard the flow, and if present, body forces. The inertial term gives a measure of the change of velocity of one fluid element as it

moves about in space. The temporal derivative gives a measure of the change of velocity at a fixed point and it is known as the local derivative. The remaining three terms of the inertial term are grouped together and known as the convective terms.

2.3.3 Energy Equation

The rate of change of energy inside the fluid element must equal the net flux of heat inside the element and the rate of working done on it due to body and surface forces. Under assumption of Newtonian, isotropic fluid and incompressible flow it can be written as:

$$\rho c_p \left(\frac{\partial T}{\partial t} + u \frac{\partial T}{\partial x} + v \frac{\partial T}{\partial y} + w \frac{\partial T}{\partial z} \right) = \frac{\partial}{\partial x} \left(k \frac{\partial T}{\partial x} \right) + \frac{\partial}{\partial y} \left(k \frac{\partial T}{\partial y} \right) + \frac{\partial}{\partial z} \left(k \frac{\partial T}{\partial z} \right) + \phi + \left(u \frac{\partial p}{\partial x} + v \frac{\partial p}{\partial y} + w \frac{\partial p}{\partial z} \right) \quad (2.14)$$

where c_p is the specific heat at constant pressure, k is the thermal conductivity, ϕ is the dissipation function.

2.4 Turbulent Flows

Most flows encountered in engineering practice are turbulent and therefore require different treatment. Differently from laminar flows, characterized by smoothly varying velocity fields in space and time and low Reynolds number, the turbulent one are highly unsteady. They show a chaotic movement of particles which results in random changes in pressure and flow velocity. As the Reynolds number increases, the non-linear advective term tends to amplify the perturbation, thereby increasing kinetic energy and pushes the flow towards hydrodynamic instability. The viscous term performs deformation work on the fluid which increases its internal energy at the expense of its turbulent kinetic energy. Thus, the viscous term has a stabilizing effect and acts as a perturbation damper.

The effects produced by turbulence may or may not be desirable, depending on the application. Intense mixing is useful when chemical mixing or heat transfer are needed; both of these may be increased by orders of magnitude by turbulence. The following sections discuss the approaches to studying turbulent flows [10].

2.4.1 Direct Numerical Simulation (DNS)

Direct Numerical Simulation approach consist in solve the Navier-Stokes equations without using any model and so without any approximation, only a discretization method is applied. This allows to know every motion of the flow, and gives detailed information about the problem. However not all these results are useful in engineering application, and since it is too expensive, often is better to use other approaches [10].

2.4.2 Large Eddy Simulation (LES)

Every vortex in turbulence has its own length, velocity and energetic content. The larger eddies are more energetic, so they effect the conservation equation in a more significant way. On this theory Large Eddy Simulation approach is based, since it treats the larger eddies with a higher accuracy with respect to the smaller. This is similar to DNS, but less costly because not every motion is solved [10].

2.4.3 RANS Equations

For engineering purposes, we are interested only in the averaged mean field and its effects, for these reasons, the most of CFD methods consider the statistically averaged equations derived from the principle of Reynolds decomposition. Every variable can be written as the sum of a time-averaged value and a fluctuation about that value:

$$\phi(x_i, t) = \bar{\phi}(x_i) + \phi'(x_i, t) \quad (2.15)$$

The two terms on the RHS are defined respectively as:

$$\bar{\phi}(x_i) = \lim_{T \rightarrow \infty} \frac{1}{T} \int_{t_0}^{T+t_0} \phi(t) dt \quad (2.16)$$

$$\phi' = \lim_{T \rightarrow \infty} \left(\frac{1}{T} \int_{t_0}^{T+t_0} \phi^2(t) dt \right) \quad (2.17)$$

Where t is the time and T is the averaging interval that must be large compared to the typical time scale of the fluctuations.

In engines, the application of these concepts is complicated by the fact that the flow pattern changes during the cycle. Also while the overall features of the flow repeat each cycle, the details do not because the mean flow can vary significantly from one engine cycle to the next. For this reason ensemble-averaging is used: the averaging is taken over a large number of sample records. Any component of the in-cylinder instantaneous velocity can be split into an ensemble-averaged velocity and an instantaneous velocity fluctuation:

$$U_i(t) = U_E(t) + u_{i,E}(t) \quad (2.18)$$

where i is referred to engine cycle. Applying Reynolds decomposition to the set of N-S equations you get the Reynolds Averaged Navier Stokes (RANS) equations. In particular the momentum equation, for the generic component, become:

$$\rho \left(\frac{\partial U}{\partial t} + \frac{\partial}{\partial x_j} (U_i U_j) \right) = - \frac{\partial P}{\partial x_i} + \frac{\partial}{\partial x_j} \left(\mu \left(\frac{\partial U_i}{\partial x_j} + \frac{\partial U_j}{\partial x_i} \right) - \rho \overline{u'_i u'_j} \right) \quad (2.19)$$

The quantity $-\overline{u'_i u'_j}$ is known as the Reynolds stress tensor, which is symmetric and has six components. Thus, by decomposing the instantaneous properties into mean and fluctuating parts, we have introduced unknown quantities, this means that the system is not closed. To close the system there are several turbulence models, among them the k- ϵ model is the most widely used turbulence model,

particularly for industrial computations and has been implemented into most CFD codes.

The modeled Reynolds stress is given by:

$$-\overline{u'_i u'_j} = 2\nu_T S_{ij} - \frac{2}{3}k\delta_{ij} \quad (2.20)$$

where ν_T is turbulent viscosity and k is turbulent kinetic energy defined as:

$$k = \frac{1}{2}\overline{u'_i u'_i} \quad (2.21)$$

According to the k - ϵ model, the turbulent viscosity is a function of turbulent kinetic energy k , its dissipation rate ϵ and a model constant which depends on the particular flow:

$$\nu_T = C_\mu \frac{k}{\epsilon} \quad (2.22)$$

Thus, in order to close the system, two additional equations are needed, one for k another one for ϵ . Respectively:

$$\frac{\partial k}{\partial t} + \bar{U}_i \frac{\partial k}{\partial x_i} = \nu_T \left(\frac{\partial \bar{U}_j}{\partial x_i} + \frac{\partial \bar{U}_i}{\partial x_j} \right) \frac{\partial \bar{U}_j}{\partial x_i} + \frac{\partial}{\partial x_i} \frac{\nu_T}{\sigma_k} \frac{\partial k}{\partial x_i} - \epsilon + \nu \frac{\partial^2 k}{\partial x_i \partial x_i} \quad (2.23)$$

$$\frac{\partial \epsilon}{\partial t} + \bar{U}_i \frac{\partial \epsilon}{\partial x_i} = C_{z1} \frac{\epsilon}{k} \nu_T \left(\frac{\partial \bar{U}_j}{\partial x_i} + \frac{\partial \bar{U}_i}{\partial x_j} \right) \frac{\partial \bar{U}_j}{\partial x_i} + \frac{\partial}{\partial x_i} \left[\left(\nu + \frac{\nu_T}{\sigma_k} \right) \frac{\partial \epsilon}{\partial x_i} \right] - C_{z2} \rho \frac{\epsilon^2}{k} \quad (2.24)$$

The model equation for ϵ is derived by multiplying the k equation by (ϵ/k) and introducing model constants.

2.5 Grid Generation and Control

Along with mathematical model, discretization method, solution method and convergence criteria, the grid's choice represent a fundamental step of simulation. The number of cell in which the domain is divided is strongly connected to the accuracy of the result and to the time required to complete the simulation. On the

one hand a fine mesh allows you to obtain detailed information of the flow, on the other this strongly increase the cost of the simulation. For this reason a trade off is necessary. In CONVERGE there are several tool which aim at controlling the grid during the simulation. For example if you are interested in the combustion in an engine, you can refine the mesh near the injector when injection occurs, while you can have a coarse one when the phenomenon is not so important for the results. In the following sections these algorithm will be presented.

2.5.1 Grid Scaling

Grid scaling allows to refine the grid at specified times, when more accurate results are needed or when critical phenomena occurs. This tool can reduce run times because the refinement is applied only for a brief period and for the rest of the simulation the grid remains coarse [8]. The grid size is changed according to:

$$scaled_grid = \frac{dx_base}{2^{grid_scale}} \quad (2.25)$$

where dx_base is the original base grid size, while $grid_scale$ in the scaling factor.

2.5.2 Fixed Embedding

Fixed Embedding is used to refine the grid at specific locations in the geometry, when a higher accuracy is needed. Moreover this refinement could be permanent or occurs only in specific period of the simulation time [8]. An example in the simulations carried out for this work, is the spark region which is small and its importance in results lasts only for few degrees (crank angle near the spark time).

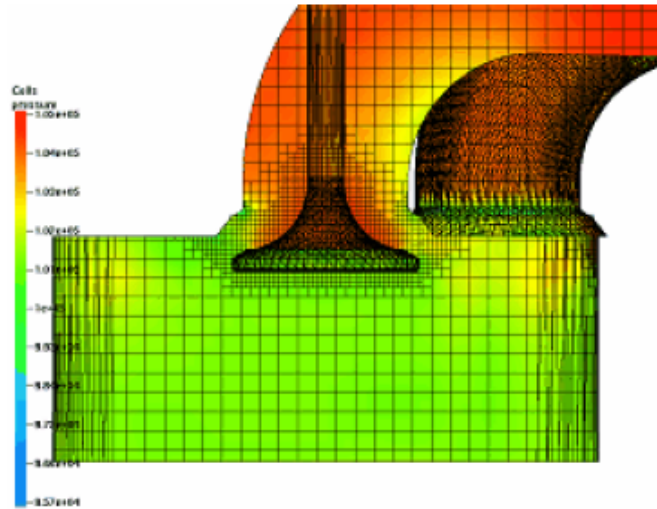


Figure 2.3. Example of Fixed Embedding around a valve [8]

It is possible to implement different kind of embedding, depending on the application:

- Boundary Embedding: it is possible to enhance the resolution near surfaces even if the moving ones. For example, it is important in the case of valves (Figura 2.3), which need to have more attention during their lift;
- Sphere Embedding: you can add a spherical region by giving radius and center;
- Cylinder Embedding: it defines a cylindrical or truncated conical area by defining center and radius of both bases;
- Nozzle and Injector Embedding: it gives a conical area around a nozzle or around all nozzles of the injector. The information needed are the two radius and the length of the cone, and the region will be placed with the same normal of the nozzle;
- Box Embedding: the region is defined by the center of the parallelepiped and half length in all the three dimensions.

- Region Embedding: this allows to refine the whole region, by specifying its ID.

2.5.3 Adaptive Mesh Refinement (AMR)

Use Adaptive Mesh Refinement (AMR) to automatically refine the grid based on fluctuating and moving conditions such as temperature or velocity. This option is useful for using a highly refined grid to accurately simulate complex phenomena such as flame propagation or high-velocity flow without unnecessarily slowing the simulation with a globally refined grid. Ideally, a good AMR algorithm will add higher grid resolution (embedding) where the flow field is most under-resolved or where the sub-grid field is the largest [8].

For a scalar, the sub-grid field is defined as the difference between the actual field and the resolved field:

$$\phi' = \phi - \bar{\phi} \quad (2.26)$$

where ϕ is the actual scalar field, $\bar{\phi}$ is the resolved scalar field, and ϕ' is the sub-grid scalar field. The sub-grid for any scalar can be expressed as an infinite series given by:

$$\phi' = -\alpha_{[k]} \frac{\partial^2 \bar{\phi}}{\partial x_k \partial x_k} + \frac{1}{2!} \alpha_{[k]} \alpha_{[l]} \frac{\partial^4}{\partial x_k \partial x_k \partial x_l \partial x_l} + \frac{1}{3!} \alpha_{[k]} \alpha_{[l]} \alpha_{[m]} \frac{\partial^6 \phi}{\partial x_k \partial x_k \partial x_l \partial x_l \partial x_m \partial x_m} + \dots \quad (2.27)$$

where $\alpha_{[k]}$ is $dx_k^2/24$ for a rectangular cell and the brackets, $[\]$, indicate no summation. Since it is not possible to evaluate the entire series, only the first term (the second-order term) in the series is used to approximate the scale of the sub-grid:

$$\phi' \cong -\alpha_{[k]} \frac{\partial^2 \bar{\phi}}{\partial x_k \partial x_k} \quad (2.28)$$

Note that the above equations can be easily generalized for a vector field, such as velocity. A cell is embedded if the absolute value of the sub-grid field is above a user-specified value. You can specify AMR with a different embedding scale and different sub-grid criterion for each condition. In addition to the field control, you can specify the time when the AMR will start and when it will end for each field, similar to fixed and boundary embedding timing control [8].

Chapter 3

Turbulent Combustion

Since almost every flow studied in engineering is turbulent, along with turbulence models (discussed in the previous section), the need of turbulent combustion models has increased, in order to solve problems with a greater accuracy.

Combustion requires that fuel and oxidizer are mixed at the molecular level. This process is deeply effected by turbulence. In fact during combustion eddies of different size develop. These vortices are different one to another both for length and velocity and their range goes to integral scale (the largest) to Kolmogorov scale (the smallest). The larger ones become more and more smaller according to a break-up process characterized by kinetic energy transfer, until all the energy is dissipated by viscosity. During this mechanism, strain and shear increase leading to a rise in the concentration gradients at the interface between reactants. For this reason the molecular mixing process is quickened and the combustion facilitated. However, if turbulence rate is too high, radicals could be brought out of the reaction zone, damaging combustion process [11]

This section deal with how turbulence modify combustion process, discuss the parameters that are most influenced by the phenomenon, explain how the scale of turbulence interact with the scale of combustion, and present the combustion model used in the simulations.

3.1 Laminar and Turbulent Burning Velocities

The laminar burning velocity s_L is defined as the velocity, relative to and normal to the flame front, with which unburned gas moves into the flame front and is transformed to products under laminar flow condition. In other words, is the propagation velocity of flame front, in direction normal to itself in relative motion with respect to unburned gas. It is a thermochemical transport quantity, which is a function of the fuel/air equivalence ratio (ϕ), as well as of temperature and pressure of unburned gas mixture.

The flame front consist in three regions as shown in Figure 3.1:

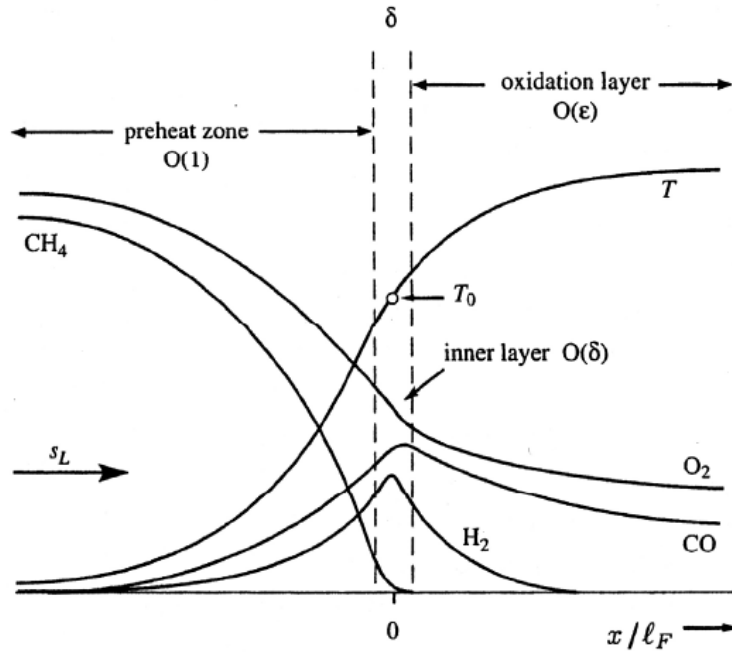


Figure 3.1. Flame Front regions

- a Preheat Zone, l , where no significant reaction or energy release occurs and the T_u , the temperature of unburned gas, is raised by the heat transfer from the chemical reaction zone. Initializing step reaction takes place, in which fuel and oxygen give radicals;

- an Oxidation Layer, ϵ , filled with hot products at the temperature of burned gas at equilibrium. This is the layer at the interface with burned gas and chain breaking reaction occurs;
- the Inner Layer, δ , a region between the other two, where the change of temperature gradients occurs thanks to chain branching reactions.

The thickness of the laminar front flame is obtained by adding these three regions:

$$L_f = l + \delta + \epsilon \quad (3.1)$$

Generally L_f is 1-2 tenths of mm, while the inner layer is about the 10% of the total.

Laminar flame speed is given by:

$$s_L = \frac{dm_b/dt}{A_f \rho_u} \quad (3.2)$$

where dm_b/dt is the mass burning rate, A_f is the front flame surface and ρ_u the unburned gas density.

3.1.1 Correlation in ICE

Laminar burning velocities at pressure typical of unburned mixtures in engines are usually measured in spherical closed vessels for different fuels (methane, propane, iso-octane, methanol, gasoline, hydrogen), pressure, temperatures and relative air-fuel ratio (RAFR). Correlations derived from these data are the most accurate means available for estimating laminar burning velocity in ICE. For example, for gasoline:

$$s_{L,0} = 0.305 - 0.549 \left(\frac{1}{RAFR} - 1.21 \right)^2 \quad (3.3)$$

where the subscript 0 suggest that s_L is evaluated at specific reference condition. For higher pressure and temperatures this correlation has to be modified:

$$s_L = s_{L,0} \left(\frac{T_u}{T_{u,0}} \right)^\alpha \left(\frac{p}{p_0} \right)^\beta (1 - 1.5x_{res}) \quad (3.4)$$

where x_{res} is the residual gas fraction of the mixture and α and β are two parameters which depend on relative air-fuel ratio. From the graph (Figure 3.2) it's easy un-

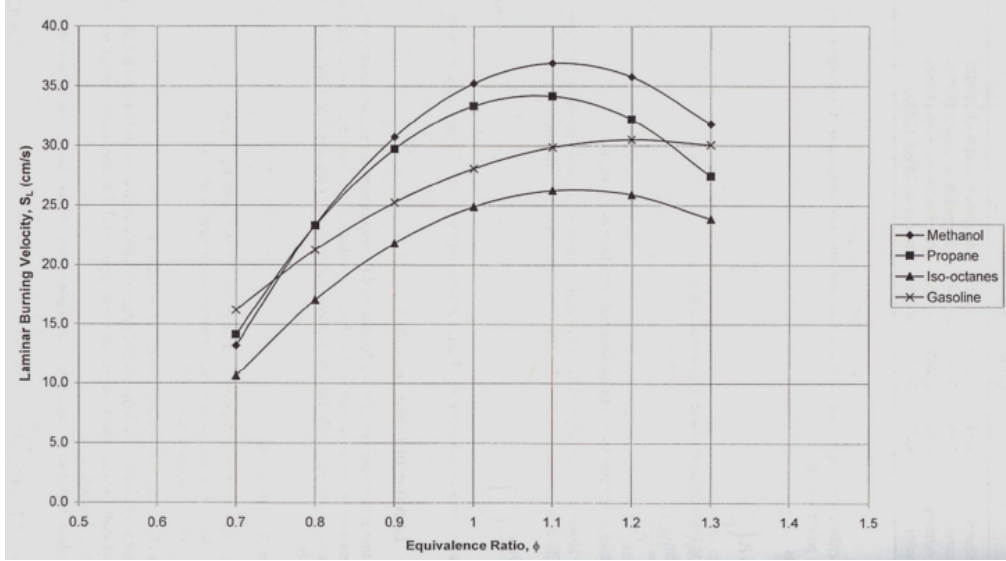


Figure 3.2. Correlation for s_L in ICE for different fuels

derstand that the maximum value of laminar flame speed is near the stoichiometric ($\phi \cong 1$). In particular, for methanol is 1.1 and for gasoline 1.2.

3.1.2 Turbulent Flame Speed

A turbulent flame speed is defined as the velocity needed at the inlet of a control volume to keep a turbulent flame stationary in the mean inside this volume [17]. There are several sub-models which aim to find turbulent flame speed starting from the laminar value. According to fractal approach:

$$\frac{A_T}{A_L} = \frac{s_b}{s_L} = \left(\frac{\epsilon_0}{\epsilon_i} \right)^{D-2} \quad (3.5)$$

where A_T and A_L are turbulent and laminar surface and D is fractal dimension of turbulent flame front. Moreover ϵ_0 and ϵ_i are respectively outer cut-off length scale and inner cut-off length scale given by:

$$\epsilon_0 = L_i = C_L(h_{min} + s_p) \quad (3.6)$$

$$\epsilon_i = \eta = L_i \left(\frac{u' L_i}{\nu} \right)^{-3/4} \quad (3.7)$$

with h_{min} the chamber clearance at TDC, s_p the linear distance of the instantaneous top of the piston from its position at TDC, C_L is a numerical coefficient, ν the unburned gas kinematic viscosity.

3.2 Regimes for Premixed Turbulent Combustion

Turbulence modify combustion because of the interaction between eddies and flame front. To describe this phenomenon, diagrams have been proposed by Borghi (1985), Peters (1986), Abdel-Gayed and Bradley (1989), Poinso et al. (1990), and many others. The diagram defines different regimes according to velocity and length scale ratio of turbulence and combustion, which indicate their interaction.

The parameters u' and L are respectively velocity and length integral scale; s_L is discussed in the previous section; the thickness L_f is given by:

$$L_f = \frac{\lambda/c_p}{\rho_u s_L} = \frac{D}{s_L} = \frac{\nu}{s_L} \quad (3.8)$$

where D is thermal diffusivity and the last equivalence is obtained under the assumption of equal diffusivities for all reactive scalars, in order to have Schmidt number equal to unity ($Sc = \nu/D = 1$). The temporal scale is the ratio between length and velocity scale.

The regions on the plot are divided by lines which refer to dimensionless number here defined:

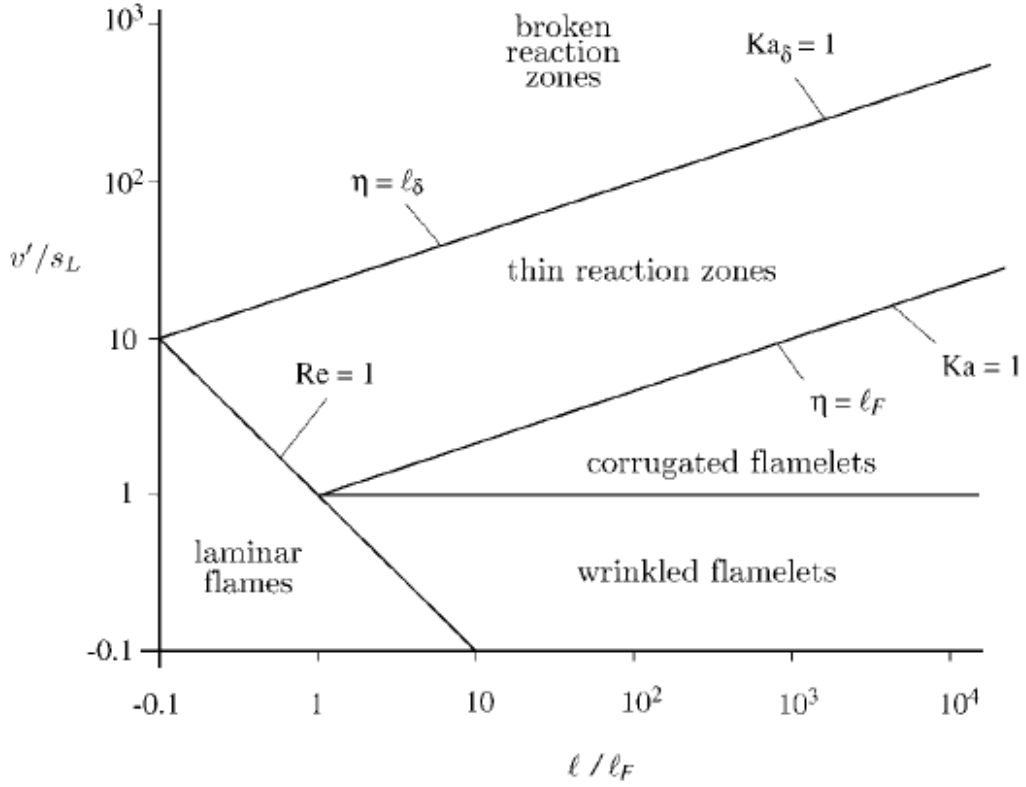


Figure 3.3. Borghi Plot

- Damköhler number, the ratio between residence and chemical time scale:

$$Da = \frac{\lambda_\tau}{t_f} = \frac{s_L L}{u' L_f} \quad (3.9)$$

- Karlovitz number, a measure of the characteristic time of laminar flame with respect to Kolmogorov turbulence time scale ($t_\eta = \eta/u_\eta$):

$$Ka = \frac{t_f}{t_\eta} = \frac{L_f^2}{\eta^2} = \frac{u_\eta^2}{s_L^2} \quad (3.10)$$

- second Karlovitz number, which consider only the inner layer thickness:

$$Ka_\delta = \left(\frac{\delta L_f}{\eta} \right)^2 = \delta^2 Ka \quad (3.11)$$

- Reynolds number for turbulence:

$$Re_T = \frac{u'L}{\nu} = \frac{u'L}{s_L L_f} = Da^2 Ka^2 \quad (3.12)$$

3.2.1 Differences between Regimes

First of all, the plot can be divided into two big zones. The one below the line $Re = 1$ holds laminar regime, while in the remaining area four different turbulent regimes are mentioned: wrinkled flamelets, corrugated flamelets, thin reaction zones, broken reaction zones.

Wrinkled flamelets are characterized by $u'/s_L < 1$. This means that the turnover velocity of all the eddies, even the largest one, is lower than the laminar flame speed. Thus, turbulence can't corrugate the flame front which propagates with the velocity s_L .

Corrugate flamelets lie between $u'/s_L = 1$ and $Ka = 1$. For this regime $s_L < u'$ but, for the restriction on Karlovitz number, $s_L > u_\eta$. Therefore there are eddies with turnover velocity equal or higher than the laminar flame speed which cause a substantial corrugation of the front. Nevertheless there is only a kinematic interaction because all the eddies are still larger than the flame front ($Ka < 1 \Rightarrow L_f < \eta$). Thus, the flame structure is not perturbed by turbulent fluctuations and remains quasi-steady.

Thin reaction zones are included between $Ka = 1$ and $Ka_\delta = 1$. The laminar flame speed of this region is lower than the turnover velocity of Kolmogorov eddies, so every eddy can corrugate the front from a kinematic point of view. Furthermore, since $Ka\delta < 1$, the thickness of flame front is bigger than the Kolmogorov length scale. By consequence these eddies can enter into the preheat zone and increase scalar mixing and expand the zone interested by thermal exchanges. However they are still bigger than inner layer (δL_f).

For $Ka_\delta > 1$, in Broken reaction zones eddies are smaller than inner layer thickness. They can penetrate and perturb it with the consequence that chemistry

breaks down locally owing to enhanced heat loss to the preheat zone followed by temperature decrease and the loss of radicals. When this happens the flame will extinguish and fuel and oxidizer will interdiffuse and mix at lower temperatures, where combustion reactions have ceased [11].

3.3 Extended Coherent Flame Model

The Extended Coherent Flame Model of Colin et al. (2003) developed to model combustion in perfectly or partially mixed mixtures is adapted to also account for unmixed combustion. The ECFM model is based on a flame surface density equation which takes into account the wrinkling of the flame front surface by turbulent eddies and a conditioning averaging technique which allows precise reconstruction of local properties in fresh and burned gases even in the case of high levels of local fuel stratification [12]. According to this model, each computational cell is divided into three zones: unmixed air zone, mixed air and fuel zone, unmixed fuel zone.

The mixing region is the one in which the model is applied. The starting point is the definition of Flame Surface Density (Σ), defined as the available flame per unit area and it is a measure of the flame wrinkling. This parameter is determined by the transport equation:

$$\frac{\partial \Sigma}{\partial t} + \frac{\partial u_j \Sigma}{\partial x_j} = \frac{\partial}{\partial x_i} \left(\frac{\mu}{Sc} \frac{\partial (\Sigma / \bar{\rho})}{\partial x_i} \right) + (P_1 + P_2 + P_3) \Sigma - D + P_k \quad (3.13)$$

where μ is the laminar viscosity, Sc Schmidt number. Moreover:

- P_1 is the flame surface production by turbulent stretch;
- P_2 models the effects of the flame thermal expansion and curvature;
- P_3 is the production by mean flow dilation;
- D is a destruction term due to consumption;

- P_k is the source term.

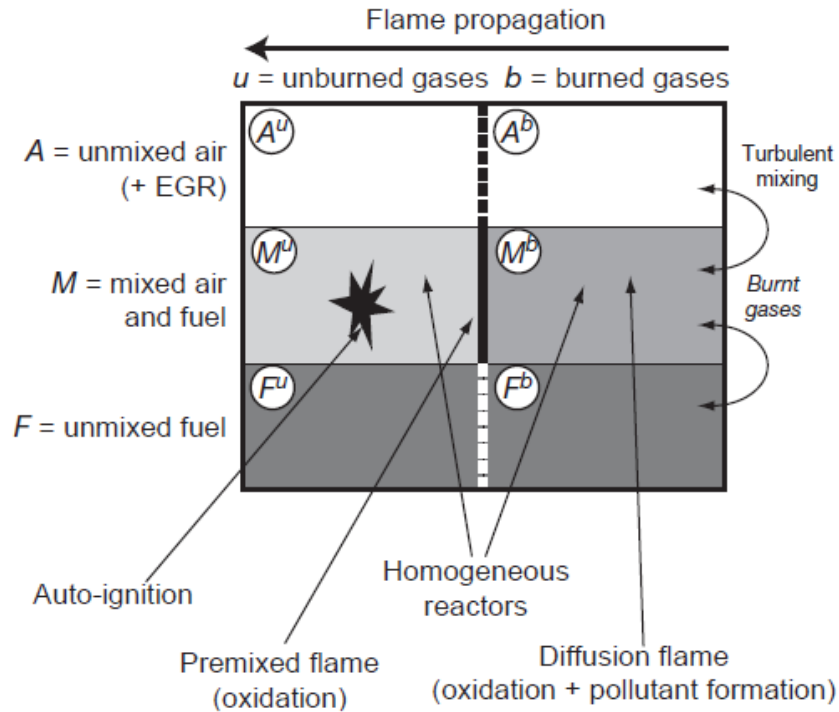


Figure 3.4. Scheme of ECFM model [12]

The model is a need to overcome some unknowns in the resolution of chemical reaction in the turbulent field, so is affected by approximation and simplification. For this reason some parameters have to be tuned in order to correctly predict the experimental behavior.

3.3.1 Flamelet assumption

The model discussed above, as many of the simulation models families, is used under the assumption of flamelet regime. With reference to Figure 3.5 "A turbulent premixed reacting flow is in a flamelet regime when a line connecting any point A in fresh gases to another point B in burnt products crosses (at least) one active flame front" [17].

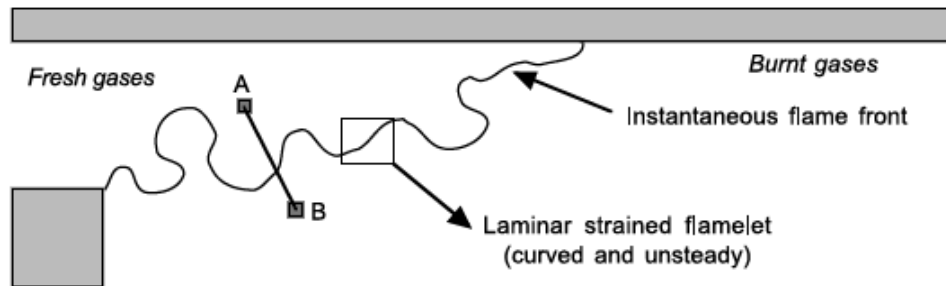


Figure 3.5. Definition of flamelet assumption [17]

Under this hypothesis, chemistry is assumed to be fast enough so that flow presents two different regions: fresh gases and burnt gases. The two parts are separated by a thin region with a laminar flame structure and in which reactions occurs. Turbulence interact with flame front and if this interaction overcome some value, this could lead to quenching phenomenon. This means that in some points combustion stops and reactants doesn't burn, so the two regions are not completely separated anymore. In this situation, the description of the reacting flow becomes much more complex and standard flamelet approaches are no longer valid.

Chapter 4

CFD Model set-up and Simulations

4.1 Simulation settings

The 3D model, implemented in the software CONVERGE, used in this work is described in Figure 4.1. It is a single cylinder, spark ignited, NG engine, in which the spark plug is represented by boundary conditions and works with a compression ratio of 13.4. The model arise from the experimental setup, in particular the length of intake and exhaust pipe depend on pressure transducer position. First aim of the simulations is to validate the model comparing results with experimental data provided by the partners of the project. Afterwards, after being calibrated, the model is used to simulate other working point, which have not been investigated with experiments, both with and without EGR.

In order to solve the governing equation, boundary conditions are required which are applied to surfaces or regions. There are different kind of boundary conditions (inflow, outflow, periodic, wall), and you can choose the nature of the boundary, if it's fixed or translating. In particular, on the intake and exhaust ports are implemented pressure and temperature data provided by experiments.

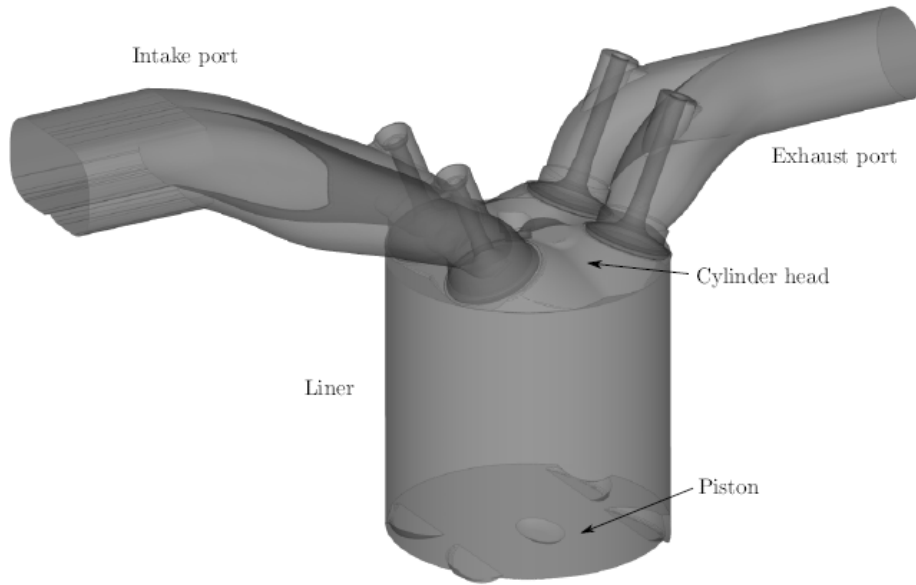


Figure 4.1. 3D Model

4.1.1 Grid settings

An interesting characteristic of CONVERGE is the automatic creation of an orthogonal, structured grid, based on grid parameters chosen by users. In this case, the base grid size is setted at 4 mm. In Section 2.5, additional tools for grid control has been discussed. The following tables list Fixed Embedding and Adaptive Mash Refinement implemented.

Table 4.1. Adaptive mash refinement

Group	Region	Scale factor
AmrGroup1	Cylinder	3
AmrGroup2	Intake Port	3
AmrGroup3	Exhaust Port	3

Table 4.2. Fixed Embedding

Region	Mode	Type	Scale factor
Cylinder	Permanent	Cylinder	2
Intake port	Permanent	Boundary	2
Intake port top	Cyclic	Boundary	3
Intake valve angle	Permanent	Boundary	3
Intake valve seat	Cyclic	Boundary	3
Piston	Permanent	Boundary	3
Cylinder Liner	Permanent	Boundary	3
Cylinder Head	Cyclic	Boundary	3
Exhaust valve top	Cyclic	Boundary	3
Exhaust valve angle	Permanent	Boundary	3
Exhaust valve seat	Cyclic	Boundary	3
Spark 1	Cyclic	Sphere	3
Spark 2	Cyclic	Sphere	3

4.1.2 Physical models

Some of the models used in simulations, have been discussed in Chapter 3. In particular for turbulence there is RNS k- ϵ model, and for combustion there are two models which work together: Extended Coherent Flame Model (Section 3.3) and Imposed Stretch Spark Ignition Model (ISSIM). This is an ignition model derived from AKTIM model (Arc and Kernel Tracking Ignition Model), from which has taken its electrical scheme. However, differently from AKTIM, allows to take in account the deformation of the surface [13]. The main purpose of the ISSIM is to simulate the reaction rate due to the flame surface density (FSD) starting at the moment of ignition, and even if it was first developed for LES, in CONVERGE can be used with RANS.

Considering Figure 4.2, which represent the inductive system, the energy stored in the primary inductance is:

$$E_p = \frac{1}{2} L_p i_p^2 \quad (4.1)$$

where L_p is inductance and i_p current.

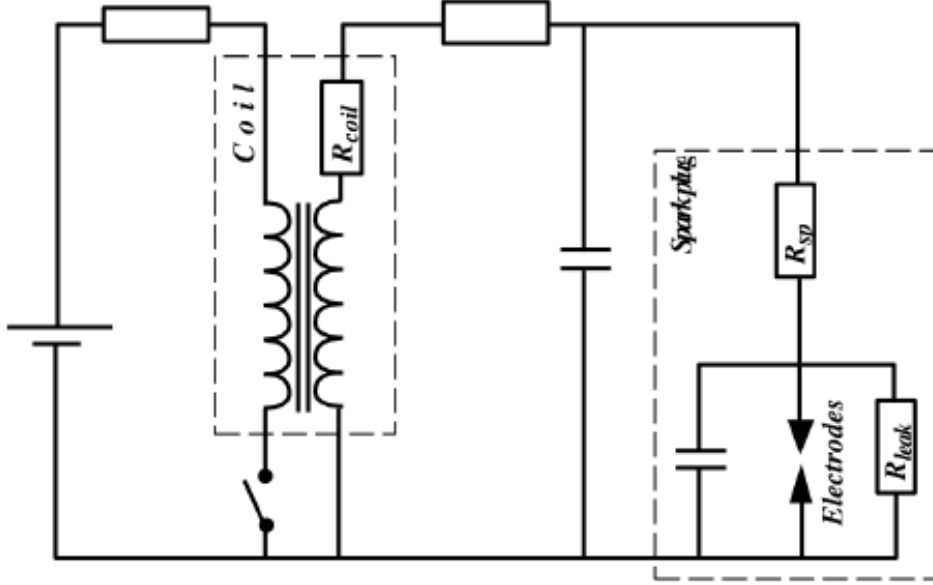


Figure 4.2. Scheme of inductive system [14]

Only about the 60% of this energy is transferred to the spark plug, the remaining part is dissipated by the secondary inductance. The life of the spark can be seen as the sum of three phases [8]: the first one is the breakdown phase. The related energy is estimated through Paschen's law [15]:

$$E_{bd} = \frac{V_{bd}}{C_{bd}^2 d_{ie}} \quad (4.2)$$

where C_{bd} is a constant and d_{ie} is the distance between the spark's electrodes.

The next phase is the glow phase, characterized by a voltage equal to the sum of cathode, anode and gas voltage:

$$V_{ie}(t) = V_{cf} + V_{af} + V_{gc} \quad (4.3)$$

The current in the secondary circuit is:

$$i_s = \sqrt{\frac{2E_s}{L_s}} \quad (4.4)$$

with E_s energy and L_s inductance. In particular, energy is given by the following equation:

$$\frac{dE_s(t)}{dt} = -R_s i_s^2(t) - V_{ie} i_s(t) \quad (4.5)$$

The total energy received by the gas is the sum of the energy received in the two phases mentioned:

$$E_{ign} = 0.6E_{bd} + \int_{t_{spark}}^t V_{gc} i_s dt \quad (4.6)$$

and the ignition occurs when this energy is higher than a critical value.

At the start of the ignition, near the spark, there is a mass of gas whose dimension depends on E_{ign} , and the initial flame kernel is assumed to be a sphere with radius r_b . The function surface density (FSD) is introduced at the start of ignition by:

$$\Sigma_{ign} = C_{surf} \frac{3\bar{c}}{r_b} \quad (4.7)$$

where \bar{c} is the burned mass volume and C_{surf} is a user-specified value (wrinkling factor). Two important parameters of these models are *alpha* (turbulent stretch coefficient) and *wrinklingfactor*, in fact they need to be chosen during the calibration of the model in order to match as well as possible the experimental data.

4.1.3 Numerical settings

The major features of time-step and PISO algorithm for numerical solution are listed in the table below.

Table 4.3. Numerical settings

Initial time-step	1e-07 s
Min. time-step	1e-10 s
Max. time-step	2e-05 s
Min. number of PISO iteration	2
Max. number of PISO iteration	9
PISO tolerance	1e-03

4.2 Model Validation

4.2.1 2000x30 NOEGR case

One point provided by experimental data is 2000x30 without EGR. For model calibration, in the simulation intake and exhaust values for pressure and temperature have been implemented. Multi-cycle simulations have been run in order to gain steady performance of the engine. Excluded the first one, which presents the higher peak, the cycles are used to calculate the Coefficient of Variation (CoV) which is compared to the experimental one. The CoV is an important instrument to evaluate the performance of the engine. To describe the stochastic nature of the problem LES should be more suitable, but has been demonstrate that also RANS is capable to capture a certain degree of variation [16].

Below is presented the final case: in cylinder pressure, average pressure, average heat release and combustion detail for each cycle.

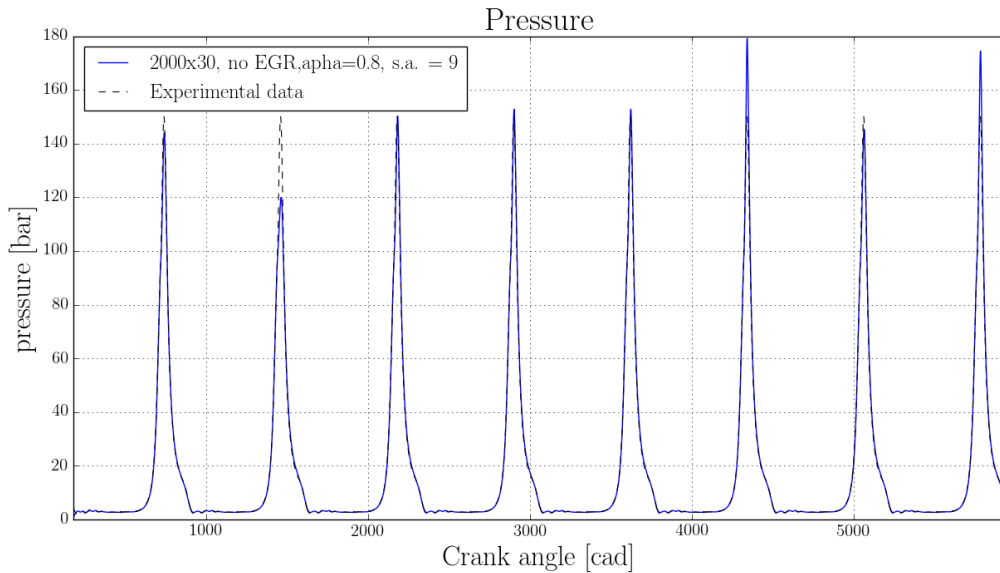


Figure 4.3. In-cylinder pressure - 2000x30 NOEGR

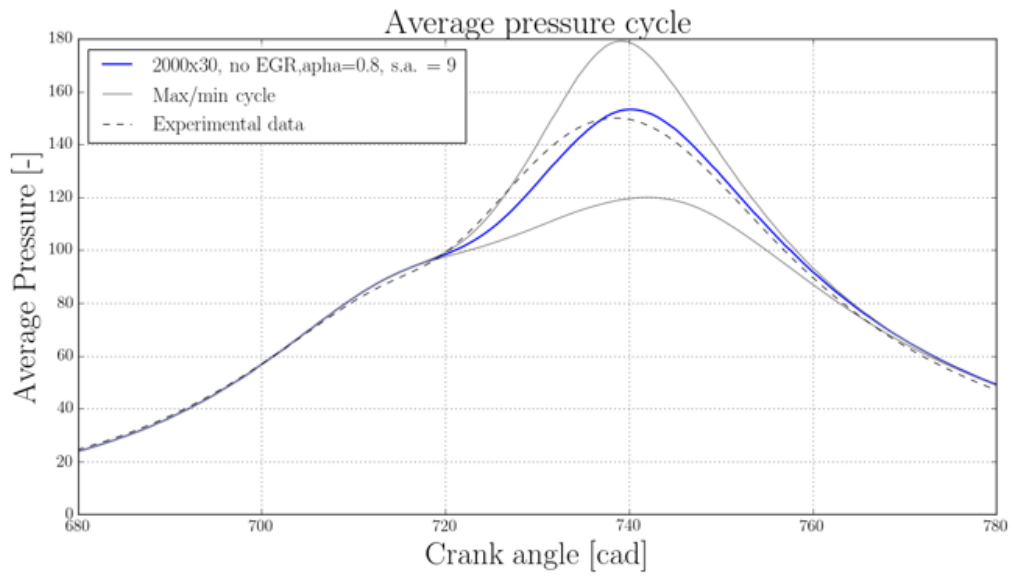


Figure 4.4. Average pressure - 2000x30 NOEGR

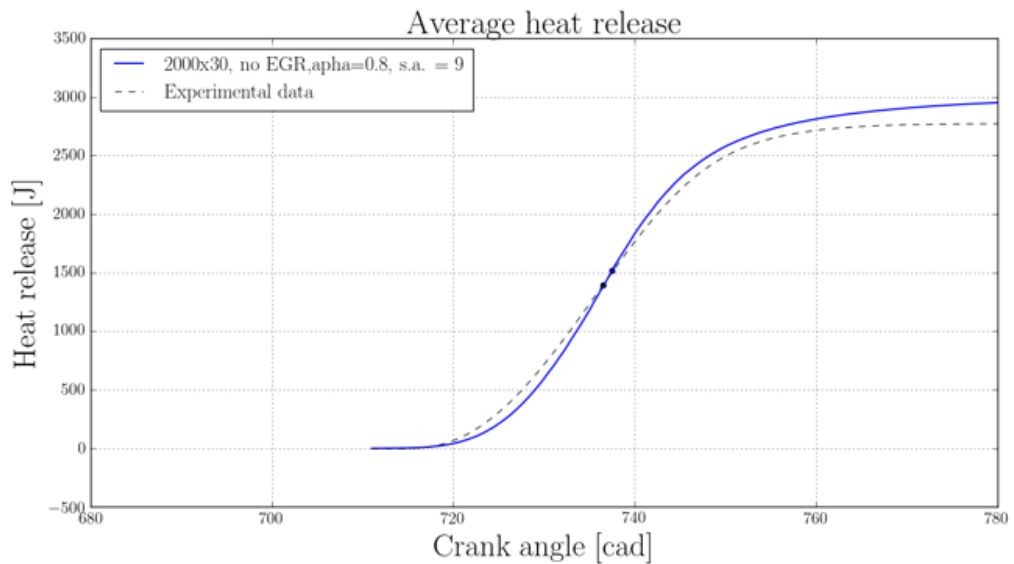


Figure 4.5. Average heat release - 2000x30 NOEGR

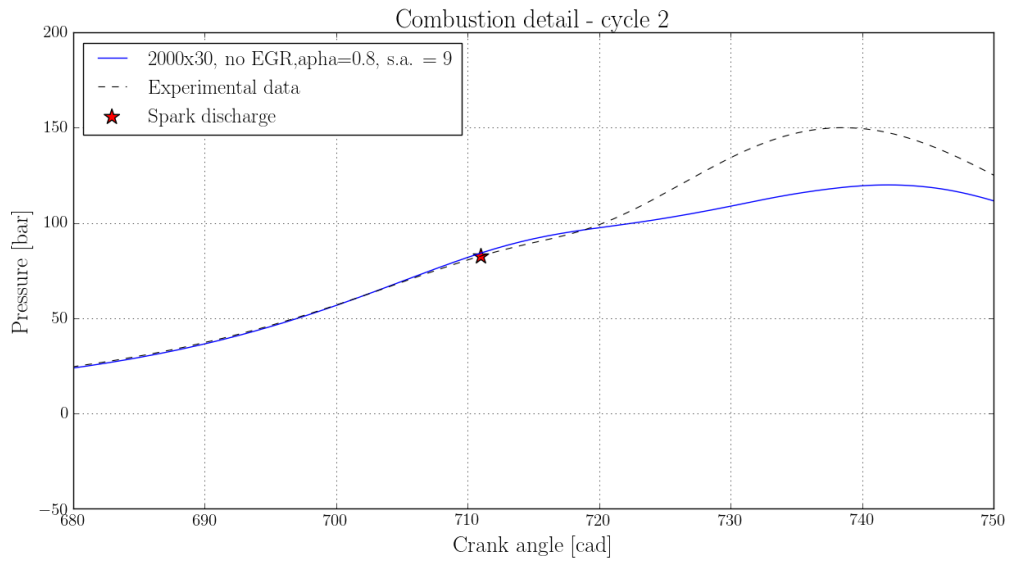


Figure 4.6. Combustion detail, cycle 2 - 2000x30 NOEGR

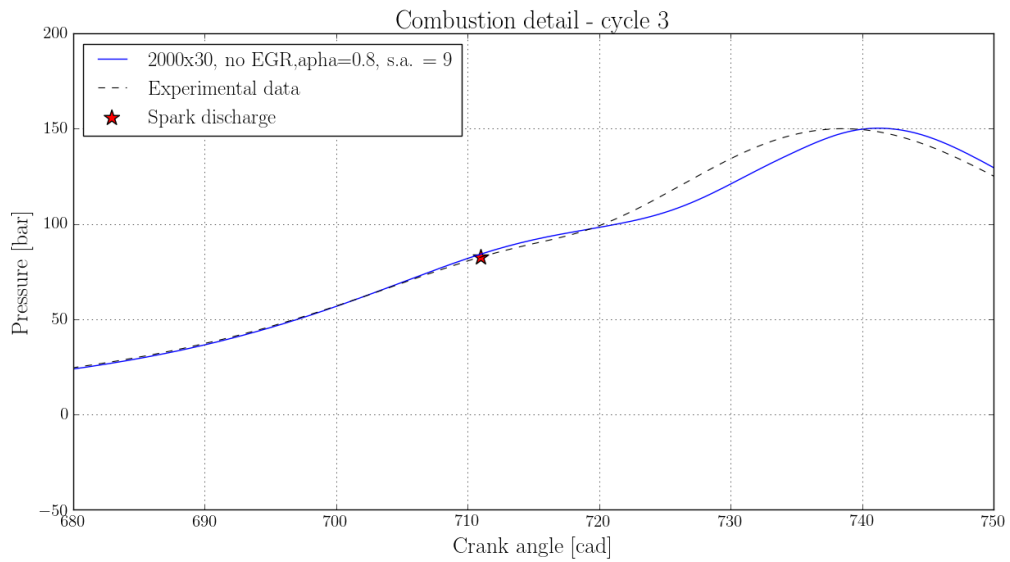


Figure 4.7. Combustion detail, cycle 3 - 2000x30 NOEGR

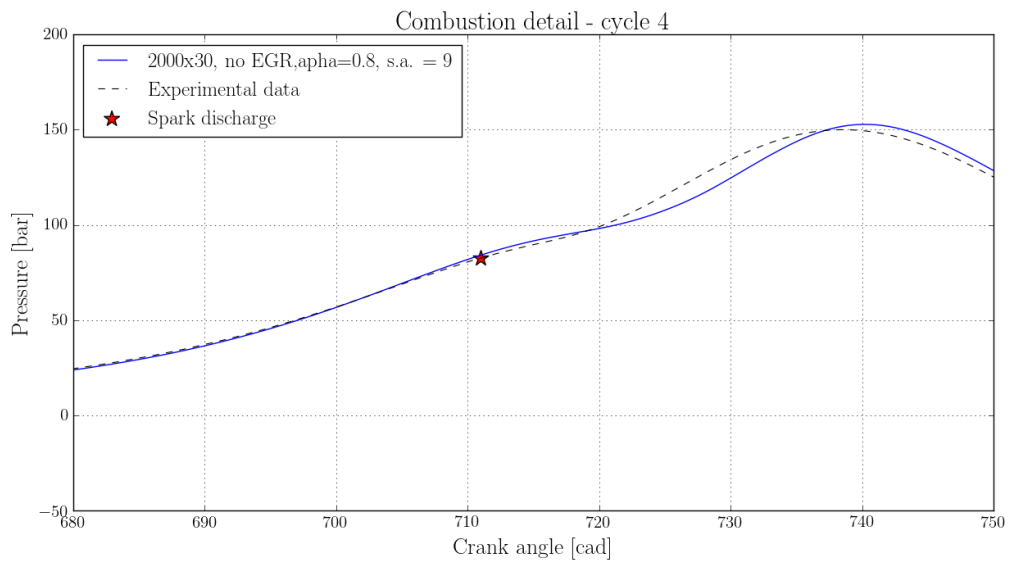


Figure 4.8. Combustion detail, cycle 4 - 2000x30 NOEGR

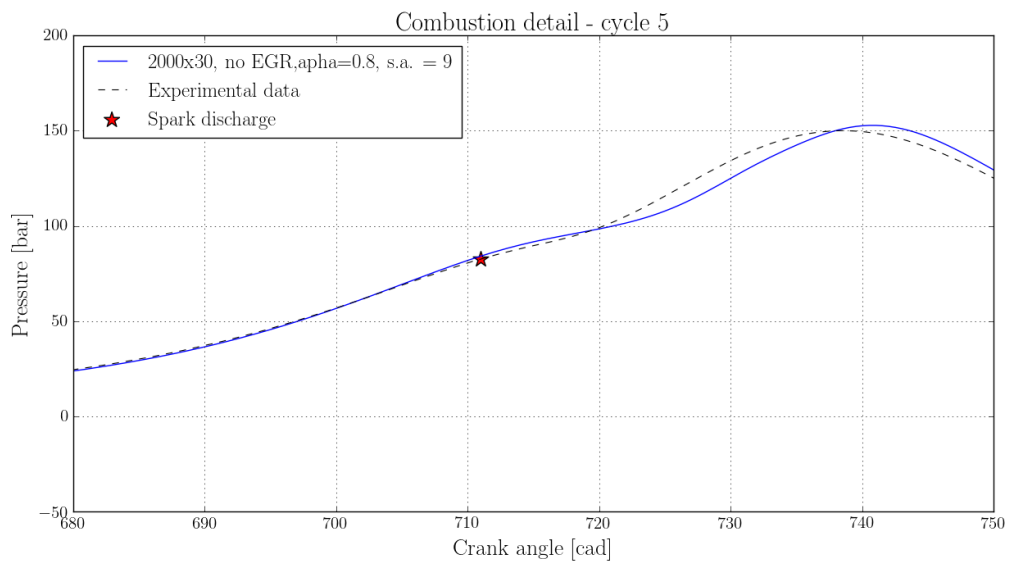


Figure 4.9. Combustion detail, cycle 5 - 2000x30 NOEGR

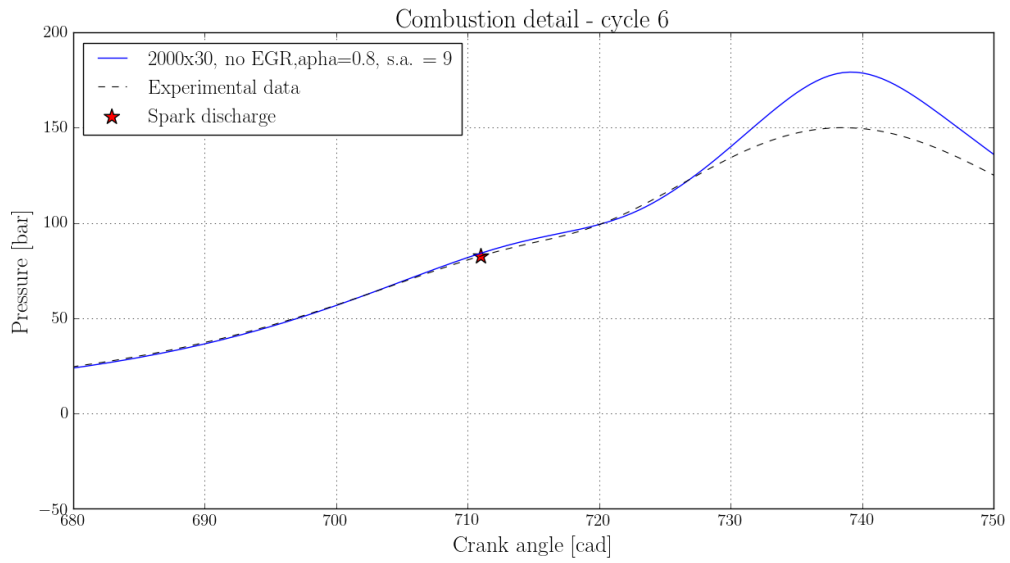


Figure 4.10. Combustion detail, cycle 6 - 2000x30 NOEGR

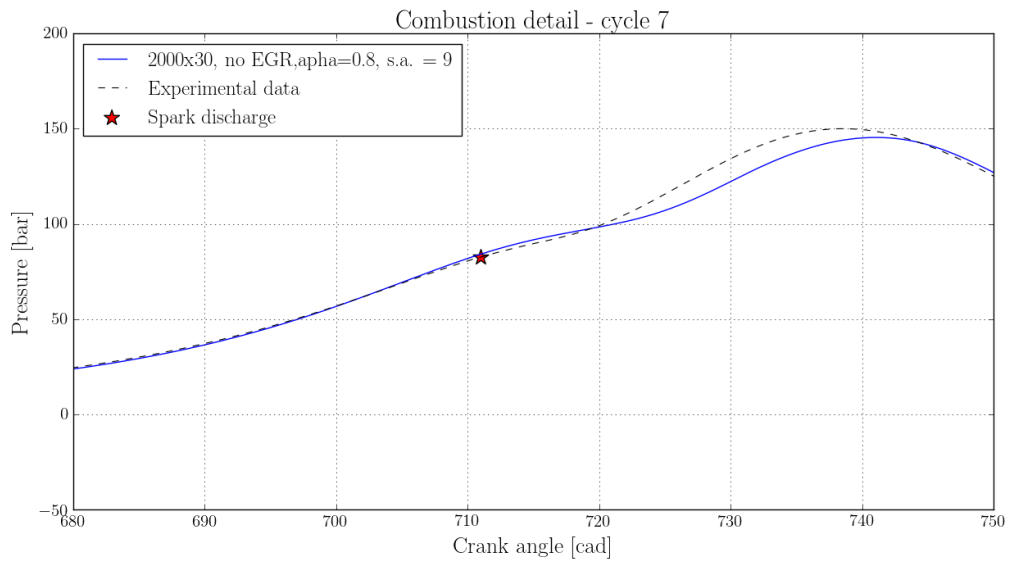


Figure 4.11. Combustion detail, cycle 7 - 2000x30 NOEGR

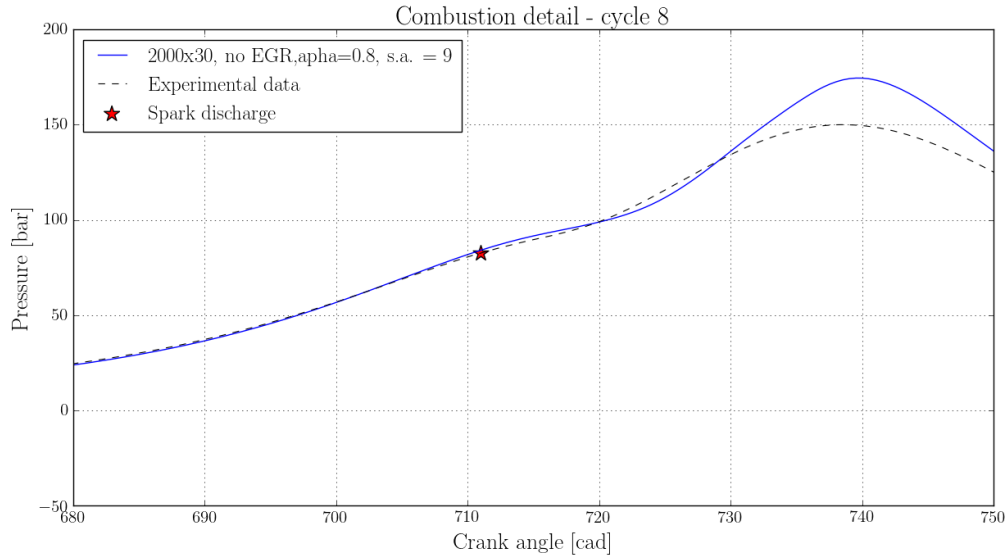


Figure 4.12. Combustion detail, cycle 8 - 2000x30 NOEGR

From combustion detail and in-cylinder pressure, it is easy to see how flow changes in the different cycles. The CoV imep of simulation is 4.02 against 2 of experimental data.

In the final case, the value of α is 0.8. The turbulent stretch coefficient is a parameter of ECFM, which multiplying the flame surface density, quickens the combustion and increases the pressure inside the cylinder. Its effect could be seen in pressure and heat release curves, comparing two cases in which only α changes.

The other calibration parameter, wrinkling factor, has been kept constant in the two tests. However, a higher wrinkling factor shifts the pressure curve up and the heat release curve to the left, which means that it leads to a higher pressure and the combustion starts earlier.

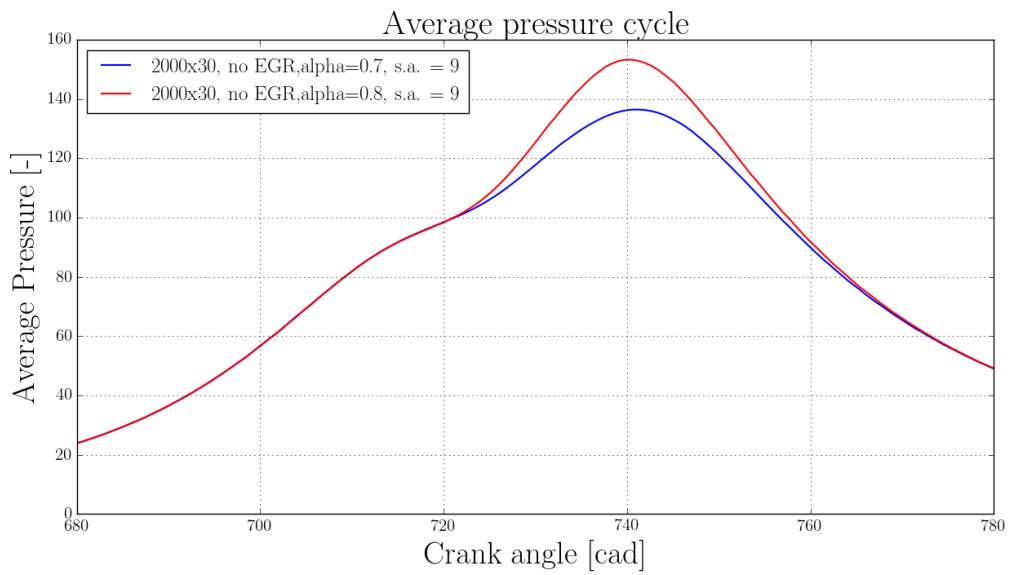


Figure 4.13. Average pressure cycle - Comparison

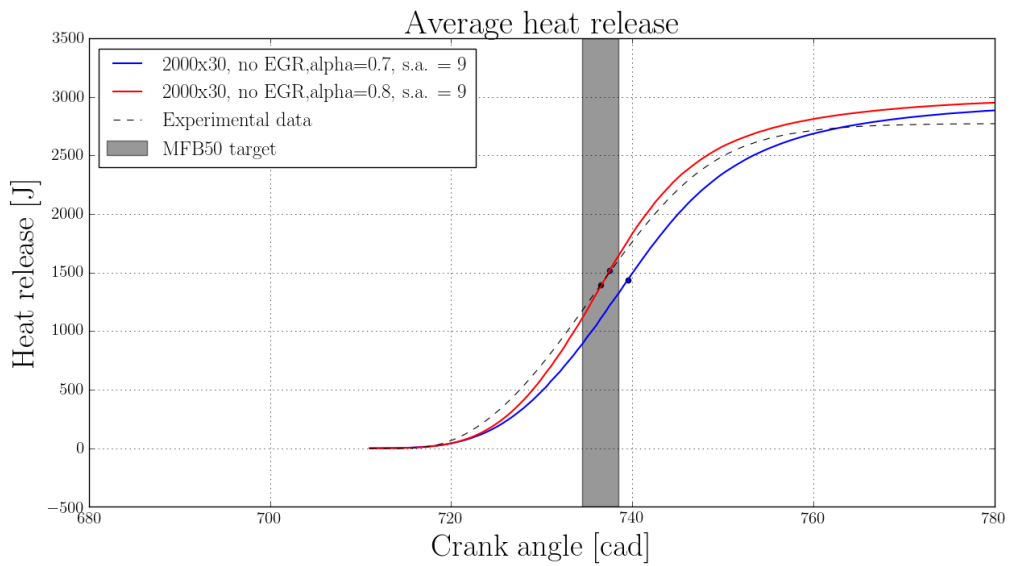


Figure 4.14. Average Heat Release cycle - Comparison

Chapter 5

EGR Sweep

5.1 EGR Sweep strategy

For simulations with different EGR rates, no experimental data were given. The strategy used in this section is summarized in the diagram below:

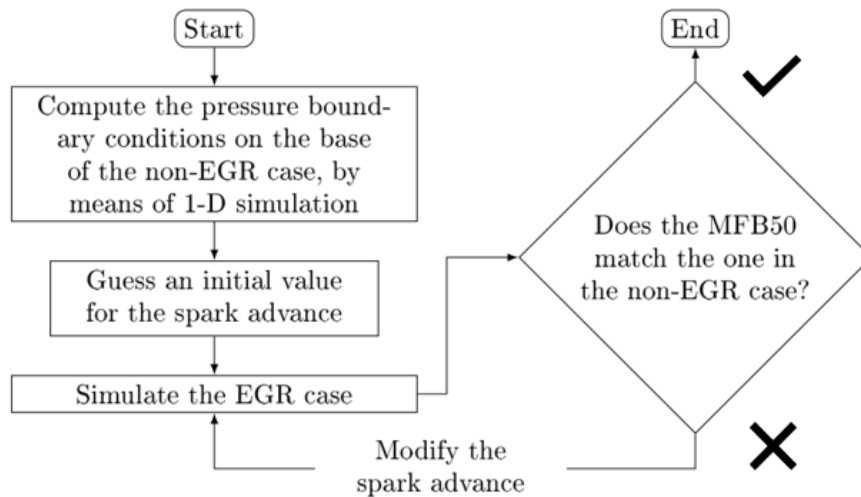


Figure 5.1. EGR Sweep strategy

The boundary condition for 3D CFD model are found by means of a 1D GT-Power model of the single-cylinder engine. For each working point, a series of

simulation with different EGR rates where performed, setting the imep value and the combustion phasing. Through this first step, boost level is defined. Then a first attempt for spark advance is made, which is needed as input for the simulations along with the boundary conditions obtained. However some changing in the set-up have to be made: in fact, in presence of EGR, exhaust gas occupy part of the cylinder, so the product of combustion are added, according to the rate of EGR setted.

In order to understand if this assumption are right, during the simulation IMEP and MFB50 are checked. MFB50 is related to the crank angle in which we have the 50% of mass burned, and the combustion phasing is supposed to be the same as no EGR cases, so a target is set on the graphs which defines a tolerance of $\pm 2degCA$. If MFB50 is out of the target the simulation is stopped and a new trial for spark advance is made. If the imep value is not the desired one, the boost level is increased or decreased by a certain percentage.

The working points investigated are listed in the table below. They are characterized by rpm x load, EGR rate and spark advance.

Table 5.1. List of all cases

rpm x load	EGR rate	Spark advance
2000x8	NO EGR	16
	20% EGR	31
	30% EGR	41
	35% EGR	46
3000x8	NO EGR	21
	30% EGR	51
2000x30	NO EGR	9
	25% EGR	11
	30% EGR	16

The bar charts below represent the different Coefficient of Variation in the final cases. For 2000x8 and 3000x8, that is at partial load, CoV imep increase as EGR

rate increase. A different behavior can be seen for 2000x30, in which for 20% of EGR, CoV is much lower than the other, and the NOEGR case results to have the higher value.

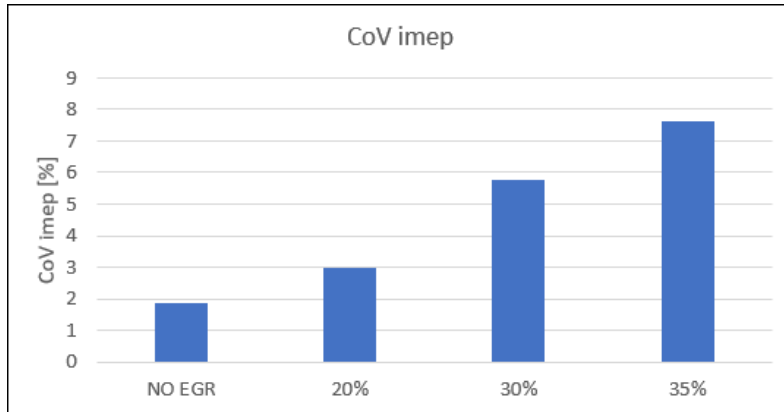


Figure 5.2. CoV imep for different EGR rates - 2000x8

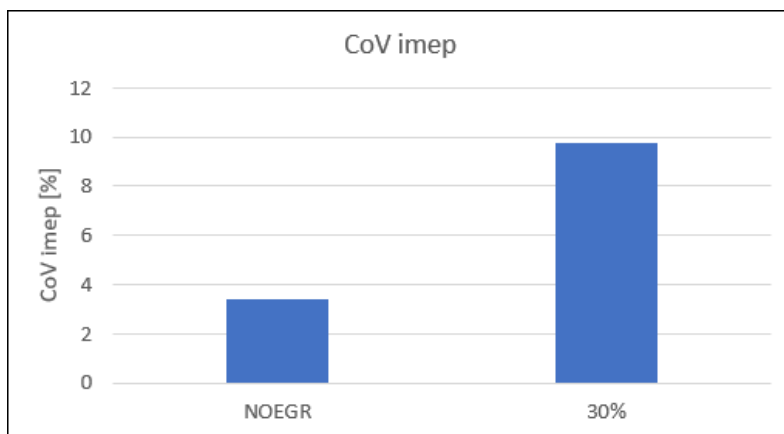


Figure 5.3. CoV imep for different EGR rates - 3000x8

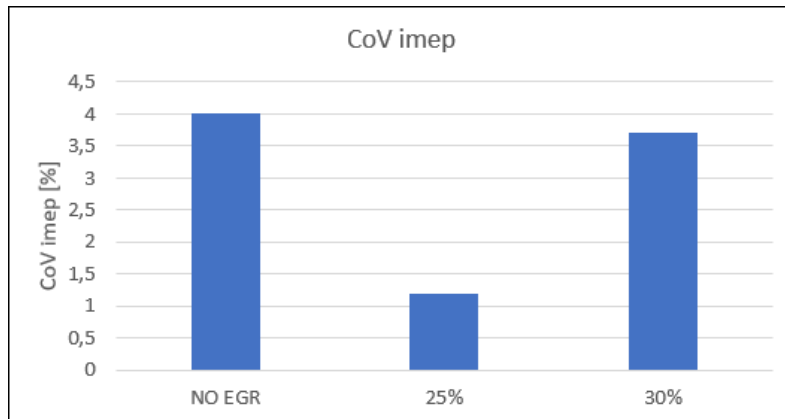


Figure 5.4. CoV imep for different EGR rates - 2000x30

A similar growing trend is found tracing a line which takes in account CoV imep values against MFB0-50 value, that is the difference between MFB50 and spark time, for different EGR rates. Generally experimental evidence are confirmed by the charts, since when burned mass reach the 50% more slowly then CoV is higher.

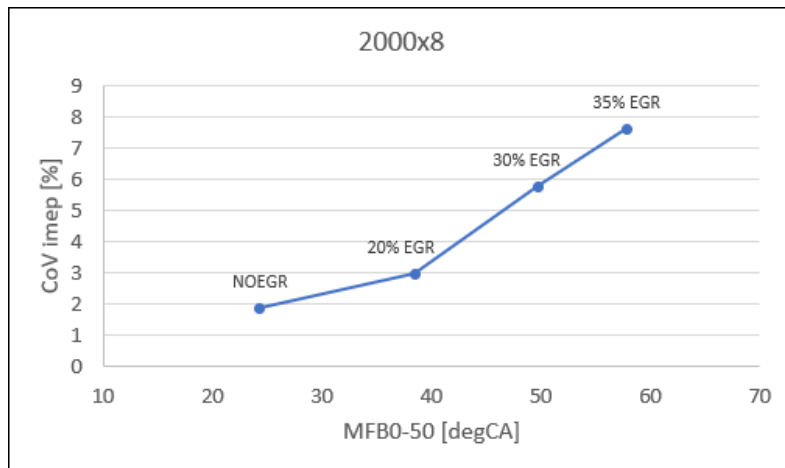


Figure 5.5. CoV imep vs MFB50 - 2000x8

Also here, the full load case has a different trend. In fact 20%EGR case has not only the lower value of CoV imep, but also of MFB0-50, while NOEGR case and 30%EGR have more or less the same value.

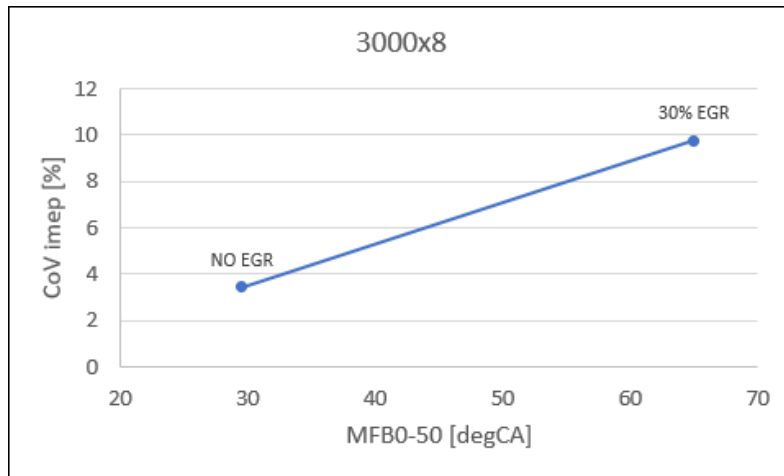


Figure 5.6. CoV imep vs MFB50 - 3000x8

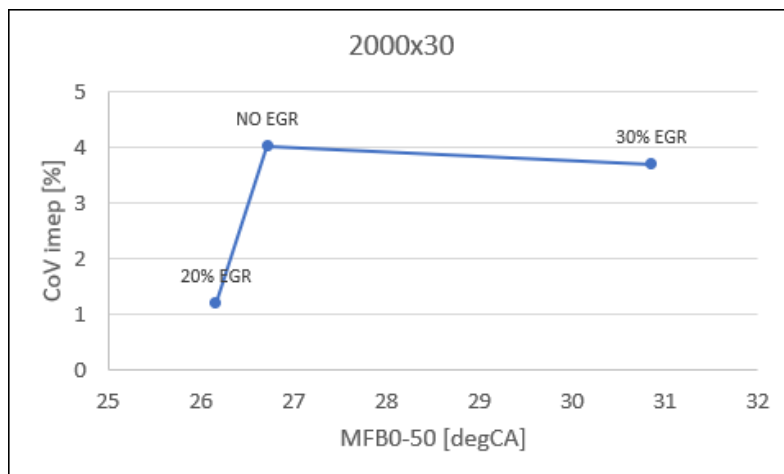


Figure 5.7. CoV imep vs MFB0-50 - 2000x30

Therefore the application of EGR dilution decrease combustion stability and increase the coefficient of variation, as confirmed by other research works [18]. Hence, a limit for dilution can be found. For example, referring to Figure 5.5, recirculating 35% of exhaust gas, leads to a CoV of about 8% that is too high for this application. It's important to identify the limit because if CoV exceed it the engine combustion stability becomes worst and some works demonstrate that the stability started to deteriorate when CoV is higher than 5% [25].

Average in-cylinder pressure and average heat release rate have been compared for all EGR cases. Looking at the pressure cycle, it's easy to see that the combustion phase is significantly different from each other, in particular as EGR content increases, the pressure is higher. In fact intake pressure in presence of EGR needs to be higher in order to reach the same load as the NO EGR case.

For what concerning heat release, the slope of the curve increases as the EGR rate increases. This mean that the combustion lasts more and the dilution decelerate the burning process.

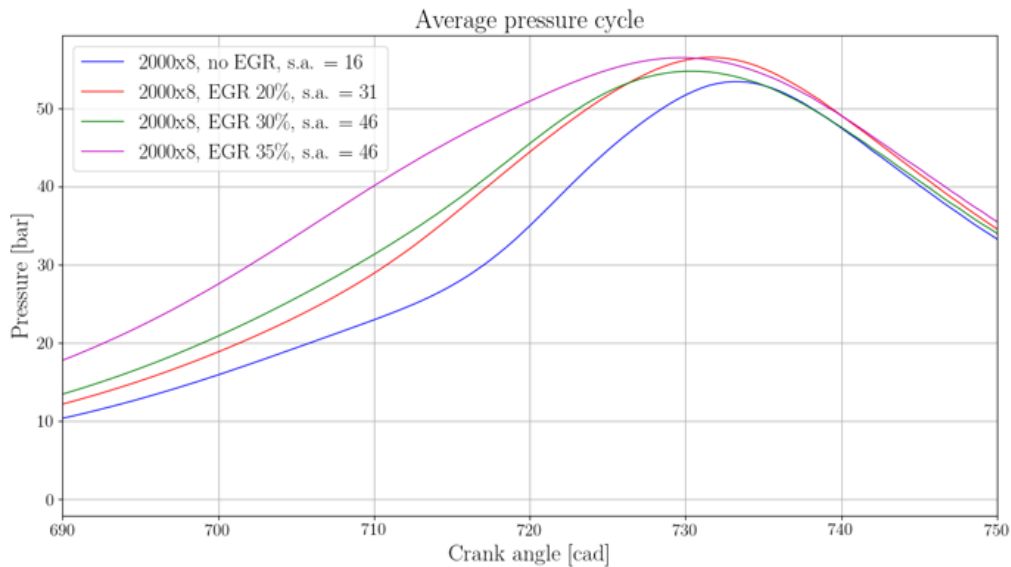


Figure 5.8. Average pressure cycle comparison - 2000x8

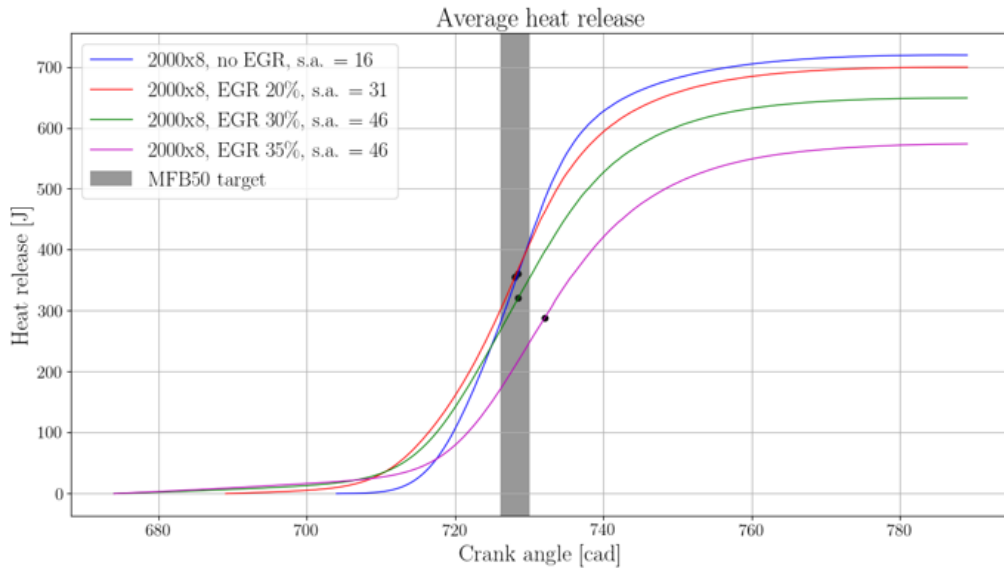


Figure 5.9. Average heat release comparison - 2000x8

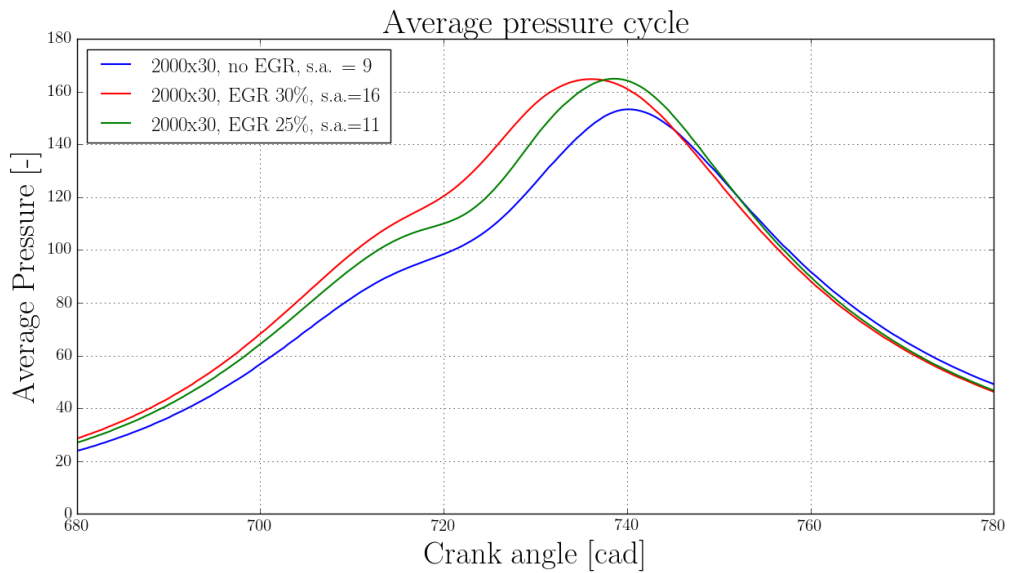


Figure 5.10. Average pressure cycle comparison - 2000x30

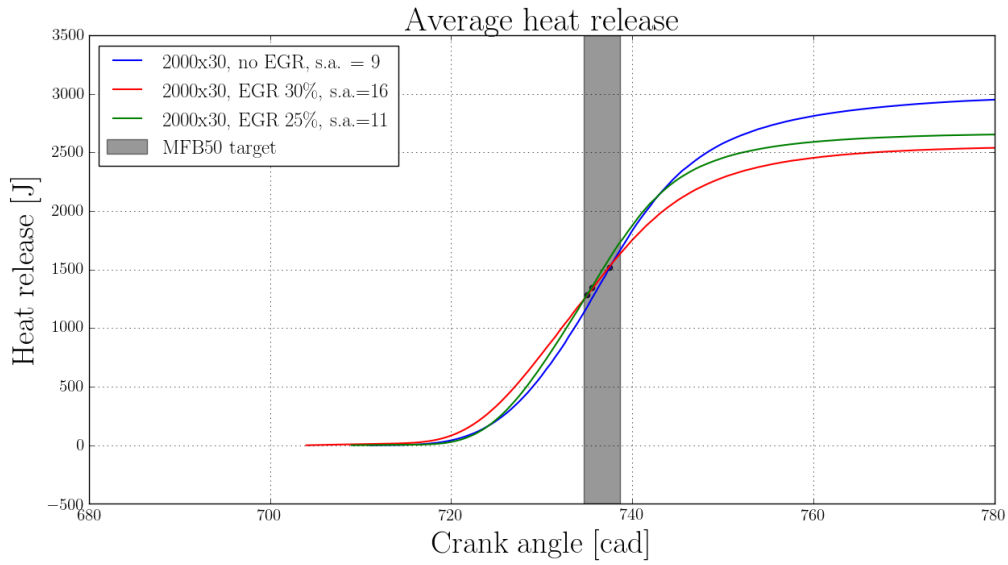


Figure 5.11. Average heat release comparison - 2000x30

Other two important parameters for engine performance evaluated are tumble and turbulent intensity. Tumble increase the turbulent level inside the cylinder, enhancing the EGR susceptibility [19]. As EGR content increase, both tumble number and turbulent intensity increase because spark advance is higher. This is confirmed by the bar graphs below, which indicates the value at SA, and the curve obtained with an ensemble average of the cycles, excluding the first one.

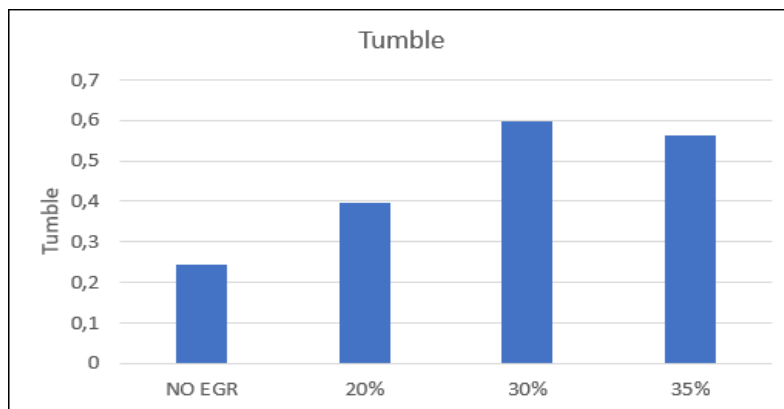


Figure 5.12. Tumble for different EGR rates - 2000x8

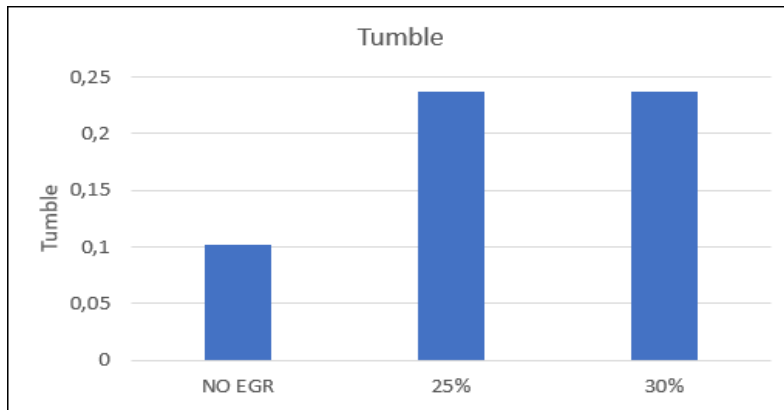


Figure 5.13. Tumble for different EGR rates - 2000x30

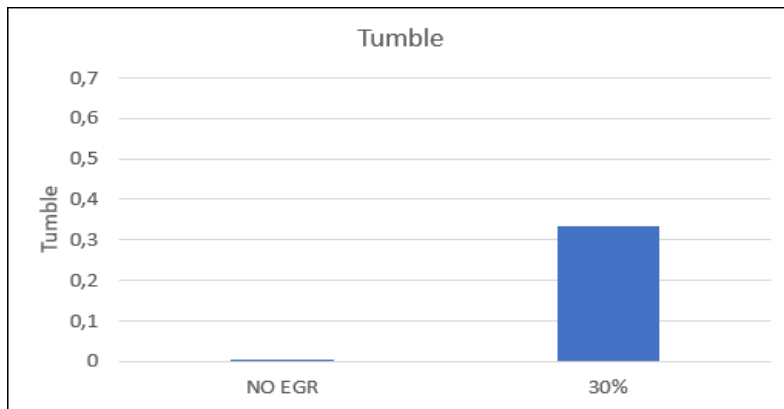


Figure 5.14. Tumble for different EGR rates - 3000x8

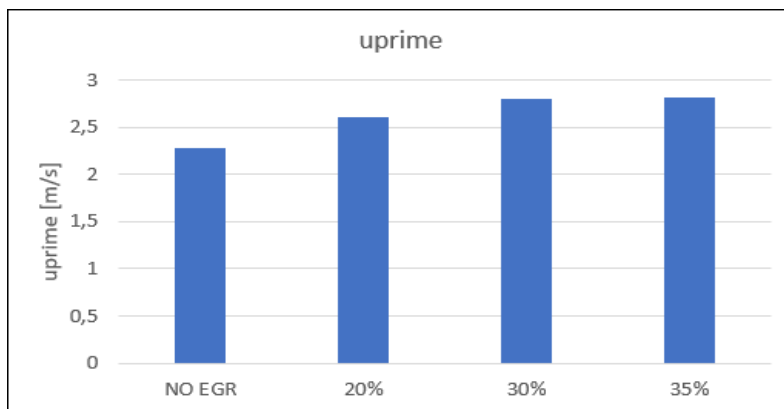


Figure 5.15. Turbulent intensity for different EGR rates - 2000x8

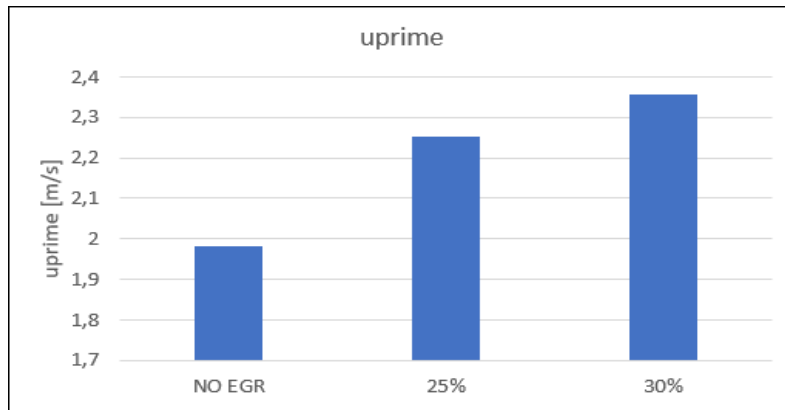


Figure 5.16. Turbulent intensity for different EGR rates - 2000x30

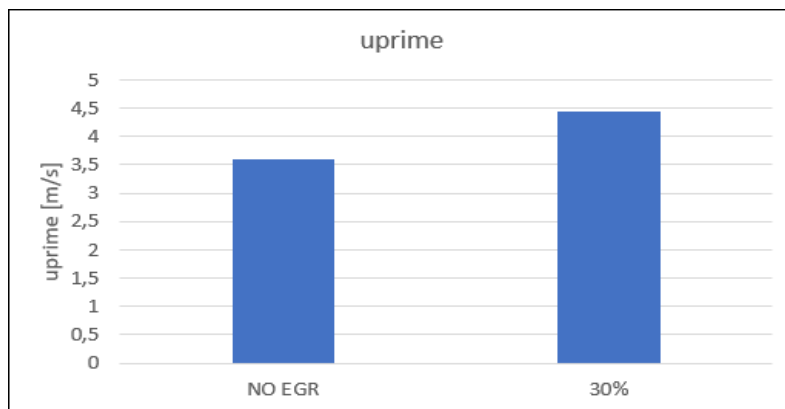


Figure 5.17. Turbulent intensity for different EGR rates - 3000x8

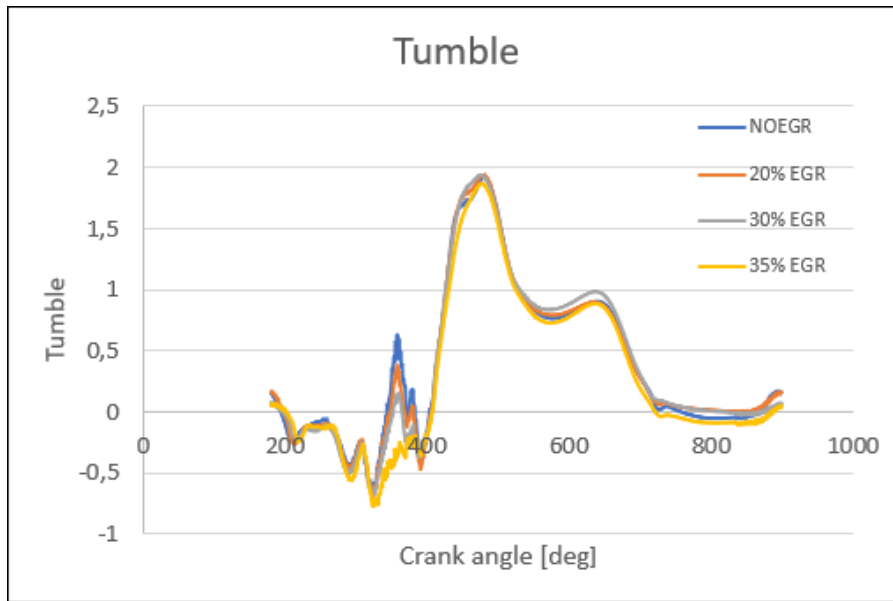


Figure 5.18. Ensemble average of Tumble - 2000x8

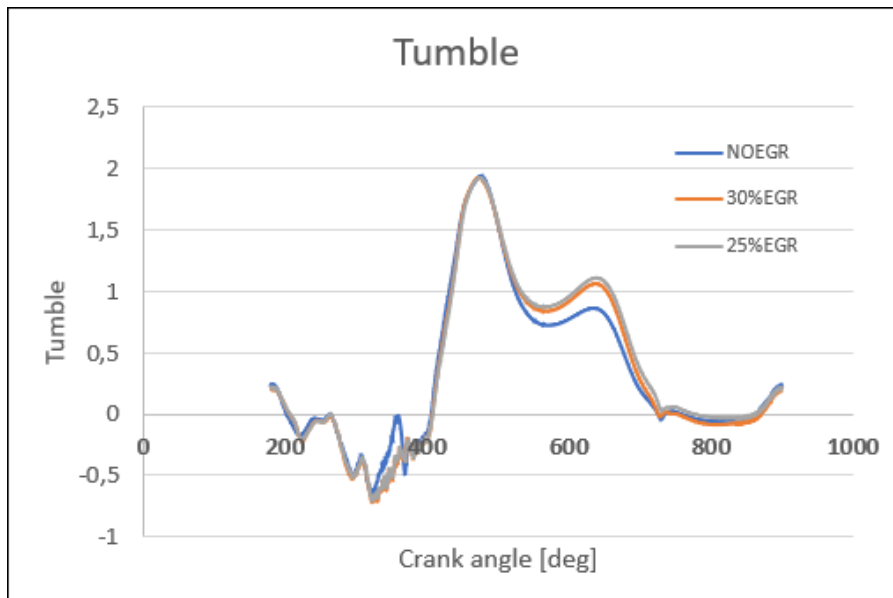


Figure 5.19. Ensemble average of Tumble - 2000x30

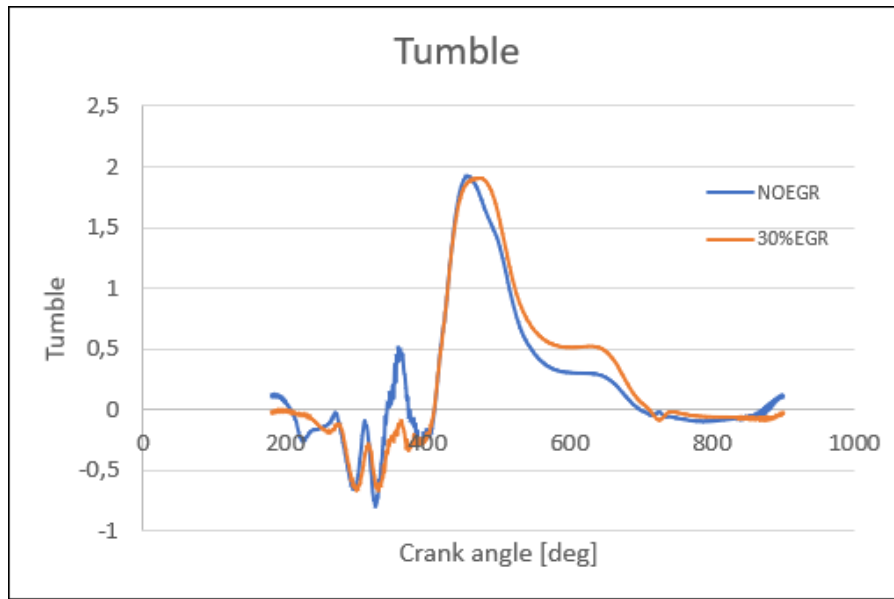


Figure 5.20. Ensemble average of Tumble - 3000x8

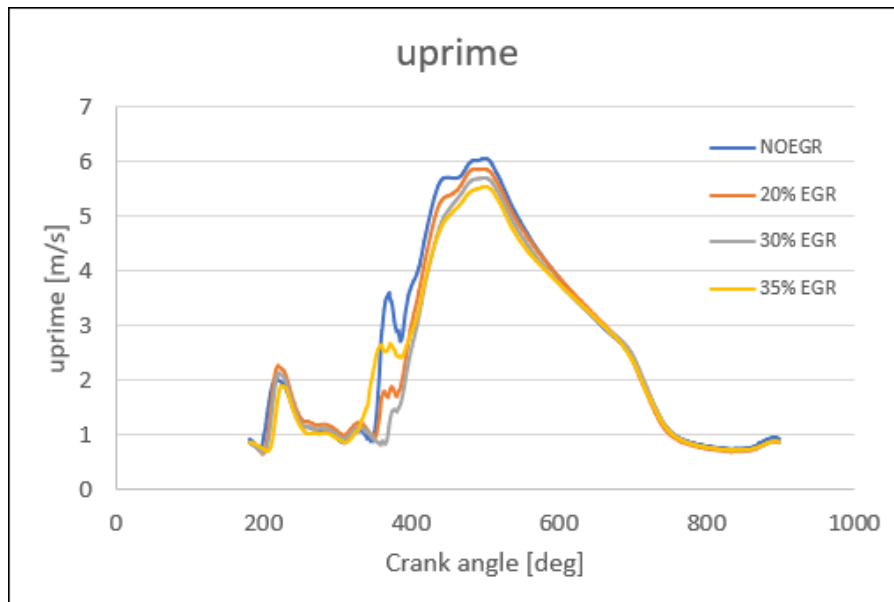


Figure 5.21. Ensemble average of turbulent intensity - 2000x8

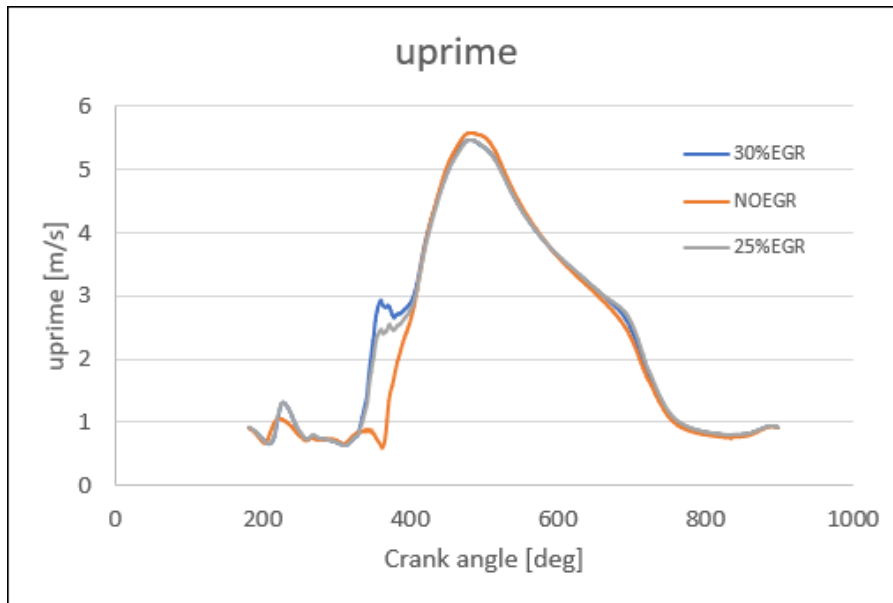


Figure 5.22. Ensemble average of turbulent intensity - 2000x30

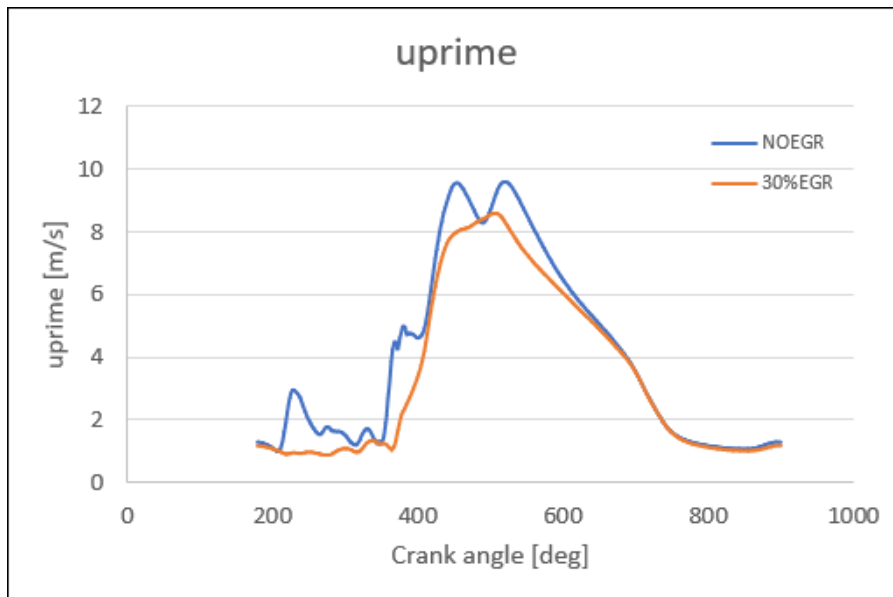


Figure 5.23. Ensemble average of turbulent intensity - 3000x8

5.2 3D Data Analysis

Exhaust gas recirculation (EGR) is an efficient method to reduce NO_x emission because it reduces the combustion temperature and oxygen concentration of the working fluid in the combustion chamber. Moreover, in SI engine, it also suppress knock combustion and enhance thermal efficiency [20],[21]. Exhaust gas displaces part of fresh air, this reduces the amount of oxygen in intake and as a consequence lower air is available for combustion and the effective air-to-fuel ratio turns to be lower. Furthermore the mixture of exhaust gas has a higher specific heat with respect to air, and this decreases the flame temperature[22]. These two factors together lead to a reduction of NO_x emissions.

Another important consideration made is about tumble. In fact a good organization of tumble in the cylinder is necessary to improve the stability of ignition and combustion of the engine. Enhancing tumble means enhancing the turbulent flow and accelerate the combustion rate. As a consequence, the combustion duration results to be smaller and the thermal efficiency higher, and this contribute to extend lean combustion limit [24]. For this reason the combination with EGR produces a significant improvements for fuel economy and a reduction in the coefficient of variation of indicated mean effective pressure. The improvement in fuel economy is the results of the reduction in pumping loss from EGR addition and improved combustion efficiency from enhanced tumble [23].

In order to have a better insight of what happen in the cylinder, an analysis of 3D data taken from simulation results was carried out. The cases 2000x8 (NOEGR and 30%EGR)and 2000x30 (NOEGR, 25%EGR and 30%EGR) where investigated, and the results are reported below.

5.2.1 y_{CH_4}

In this section, there is the comparison of the fuel concentration for the different cases at about the same crank angle after the spark time. For both 2000x8 and 2000x30, in absence of EGR combustion is faster, as stated in the section before. In fact, for each crank angle considered, the region in which burned gas are present has a bigger size with respect to EGR cases. Obviously, it's easy to compare the cases with different load. At full load, the combustion is almost finished at 40 degCA after spark, for both without EGR and with EGR figures. On the contrary, there are residual methane for 2000x8 with 30% EGR case at the same CA.

2000x8

About 10 degCA after spark:

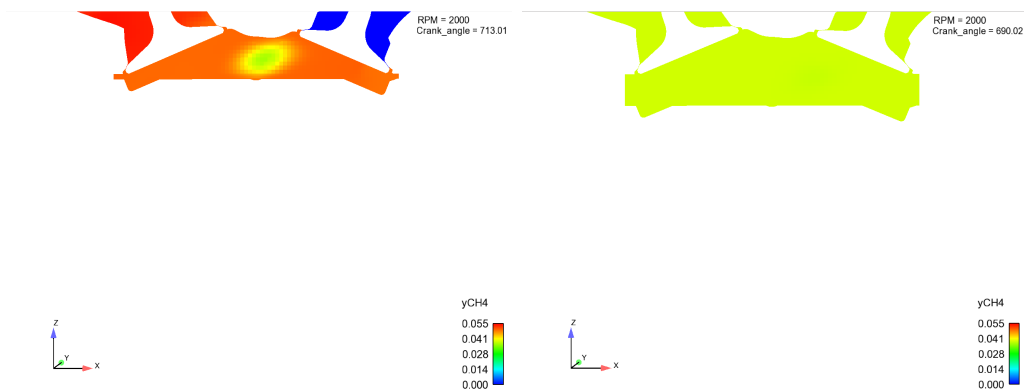


Figure 5.24. CH_4 at 10 degCA after spark - 2000x8

About 20 degCA after spark:

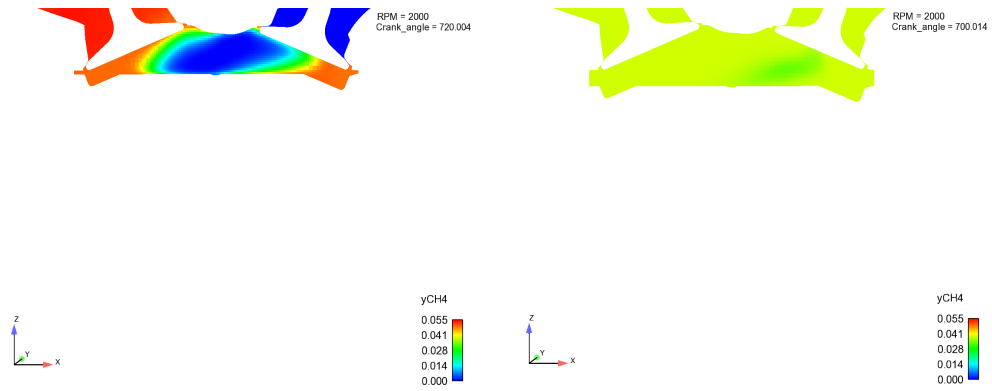


Figure 5.25. CH4 at 20 degCA after spark - 2000x8

About 30 degCA after spark:

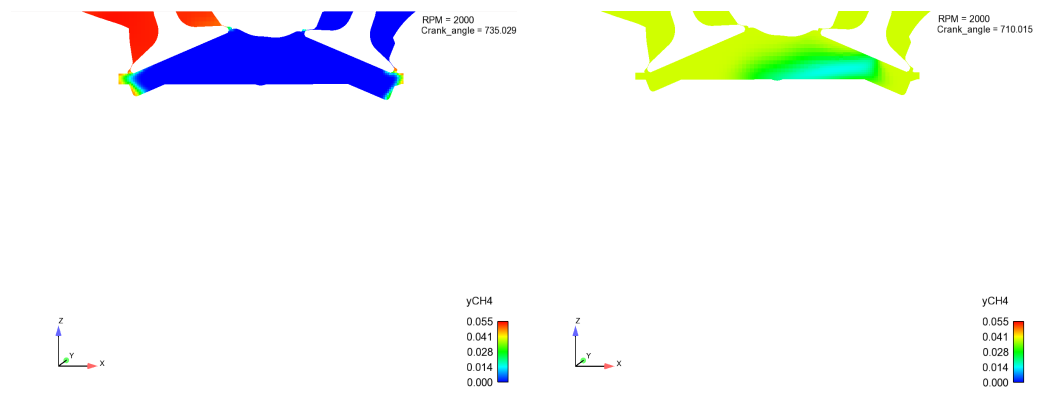


Figure 5.26. CH4 at 30 degCA after spark - 2000x8

About 40 degCA after spark:

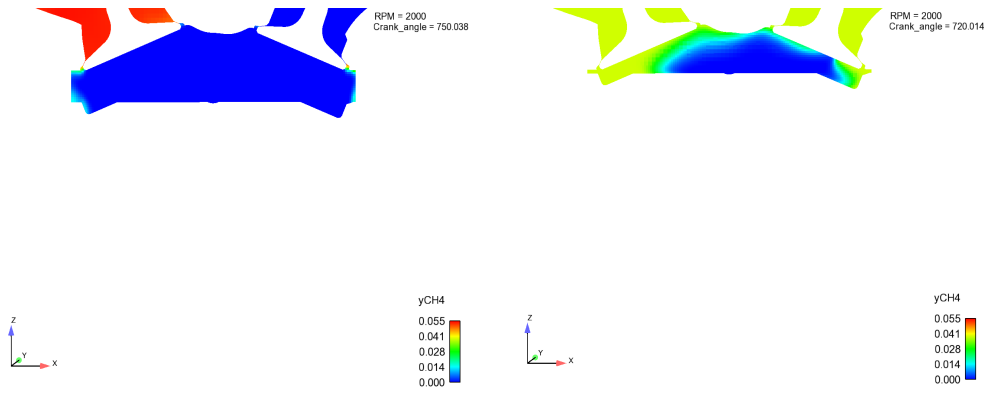


Figure 5.27. CH4 at 40 degCA after spark - 2000x8

2000x30

About 10 degCA after spark:

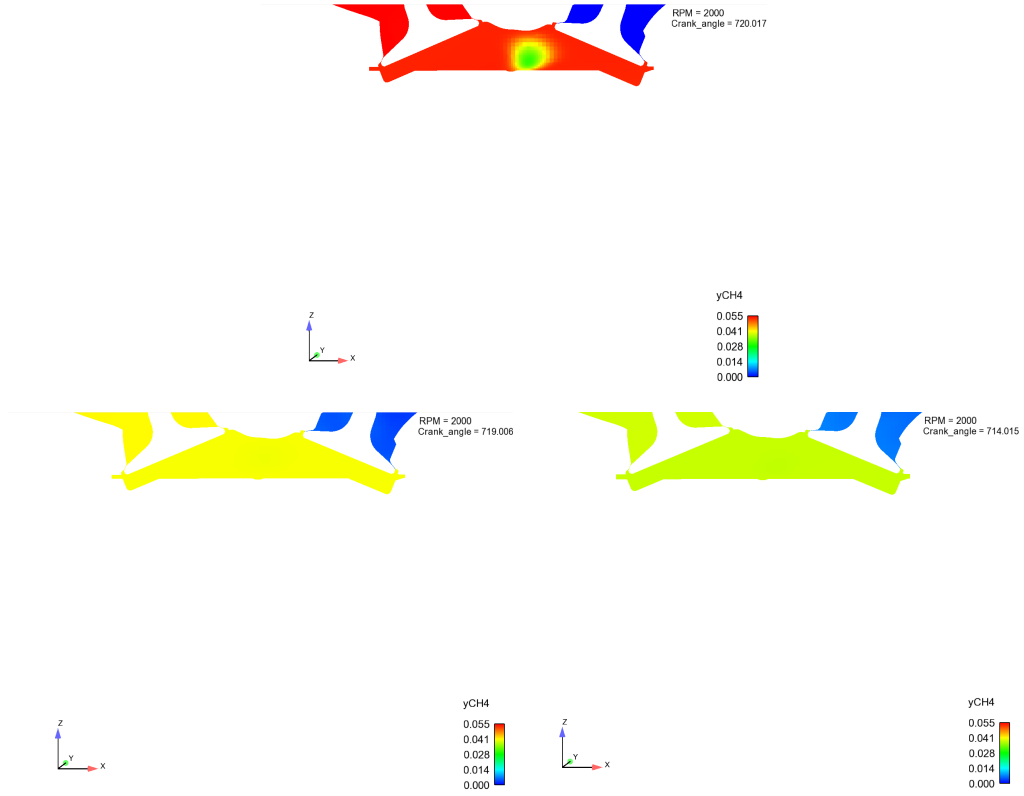


Figure 5.28. CH4 at 10 degCA after spark - 2000x30

About 20 degCA after spark:

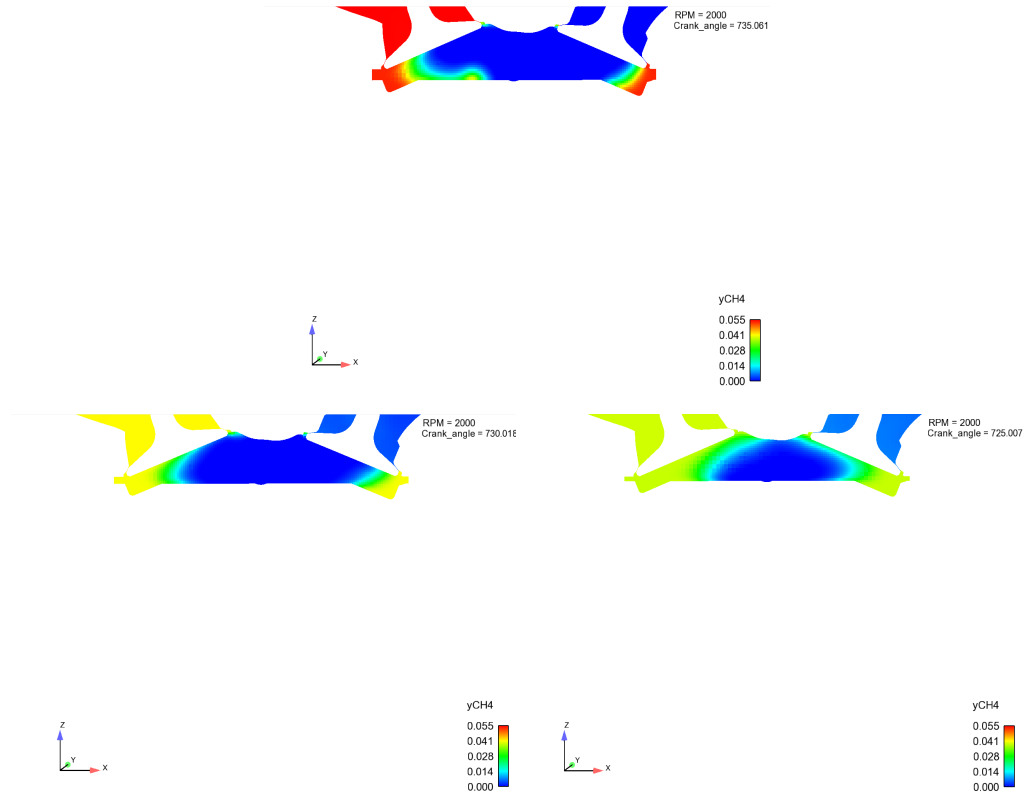


Figure 5.29. CH4 at 20 degCA after spark - 2000x30

About 40 degCA after spark:

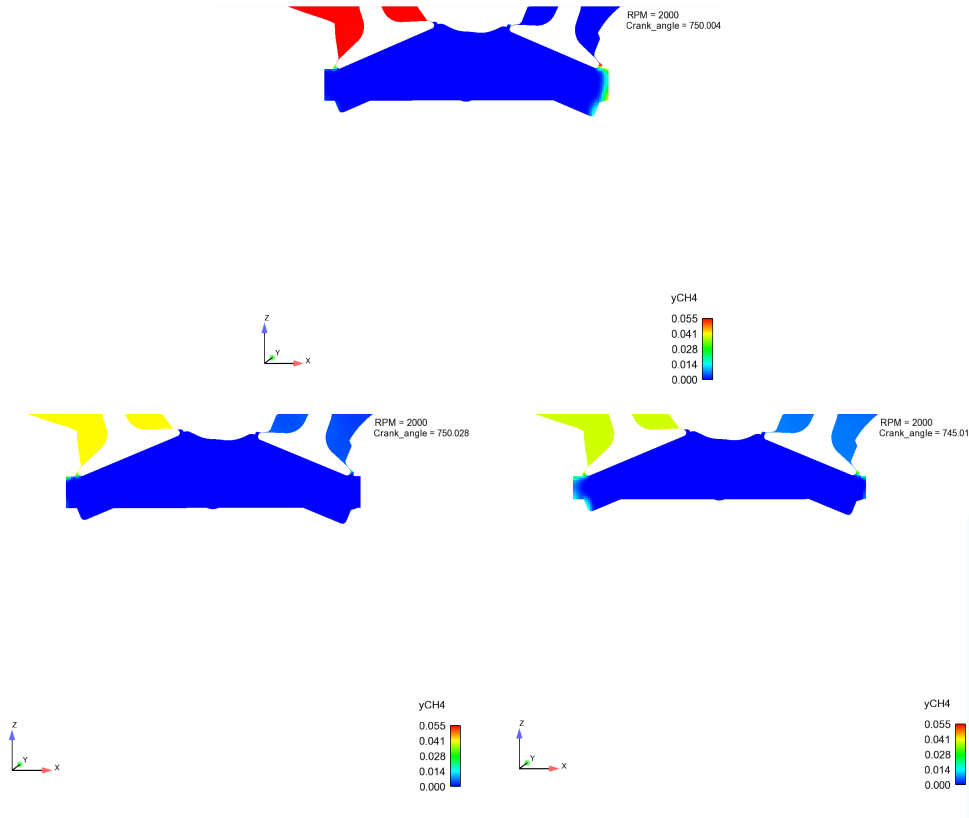


Figure 5.30. CH4 at 40 degCA after spark - 2000x30

5.2.2 Temperature

As previously said, diluted combustion leads to lower combustion temperature which in turn, gives lower NO_x emission, and this is a great advantage of this strategies. Besides, adding EGR, exhaust temperatures become minor, and this is important for the match with turbine. This results in a higher efficiency of the engine.

2000x8

About 5 degCA before spark:

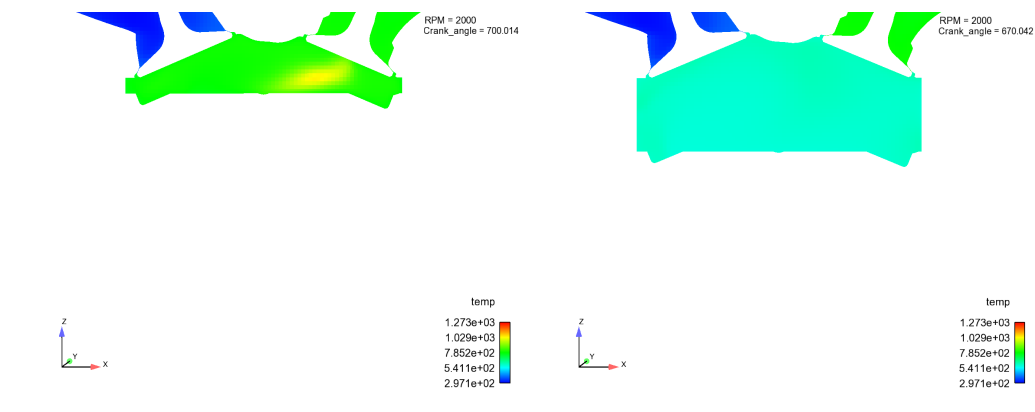


Figure 5.31. Temperature at 5 degCA before spark- 2000x8

At spark advance:

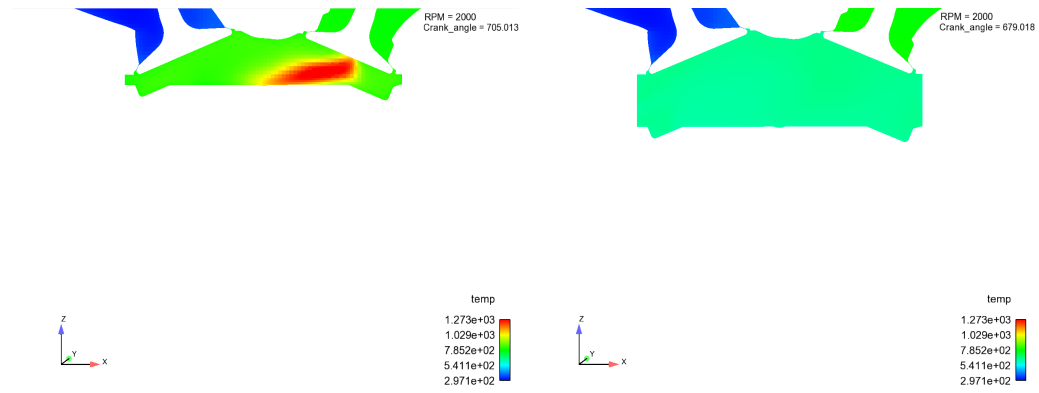


Figure 5.32. Temperature at spark advance- 2000x8

About 5 degCA after spark:

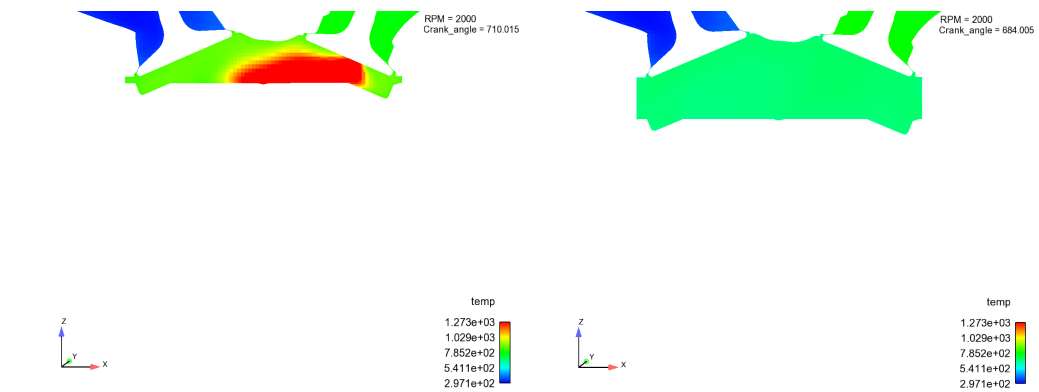


Figure 5.33. Temperature at 5 degCA before spark- 2000x8

At 840 degCA:

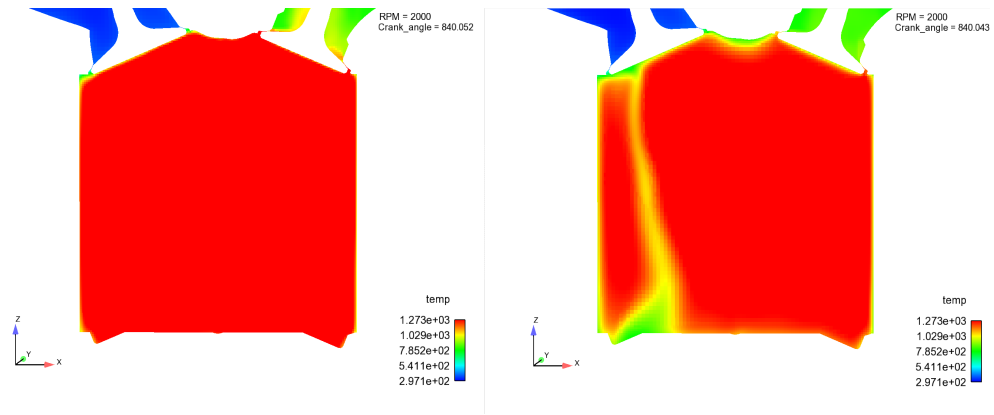


Figure 5.34. Temperature at 840 degCA - 2000x8

At 885 degCA:

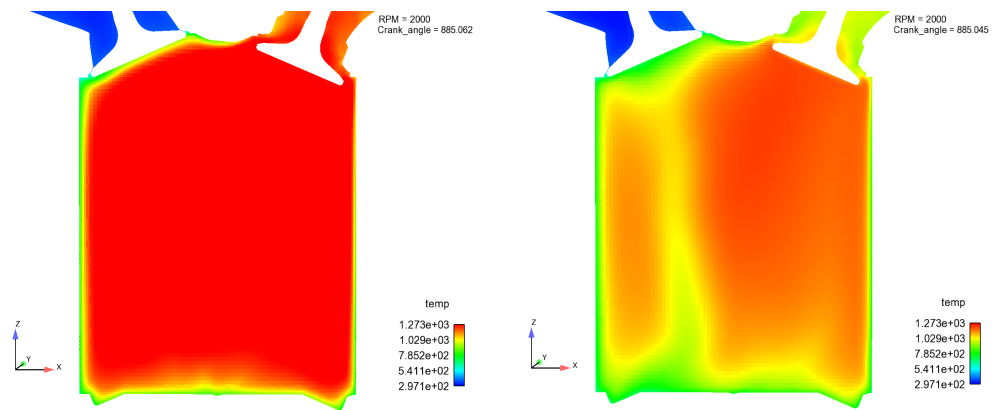


Figure 5.35. Temperature at 885 degCA - 2000x8

At 900 degCA:

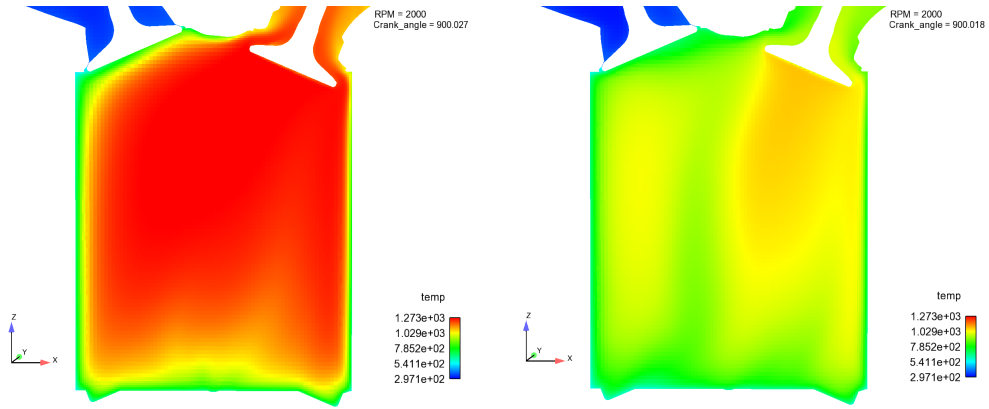


Figure 5.36. Temperature at 900 degCA - 2000x8

At 930 degCA:

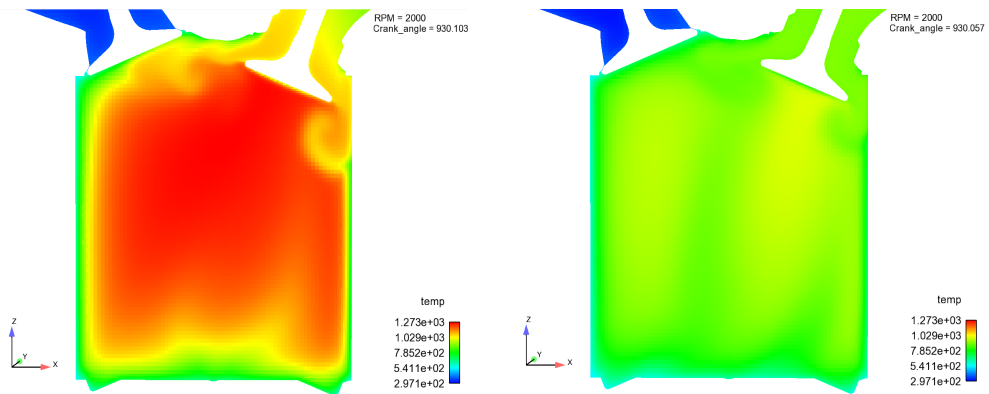


Figure 5.37. Temperature at 930 degCA - 2000x8

At 960 degCA:

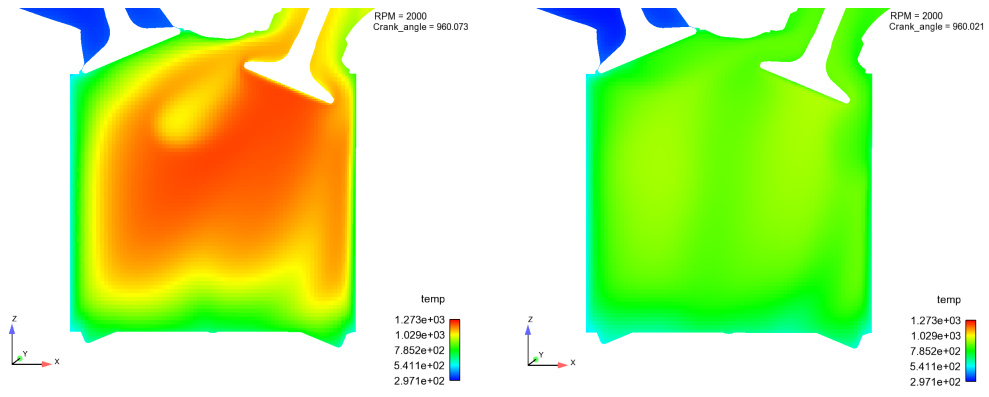


Figure 5.38. Temperature at 960 degCA - 2000x8

2000x30

About 5 degCA before spark:

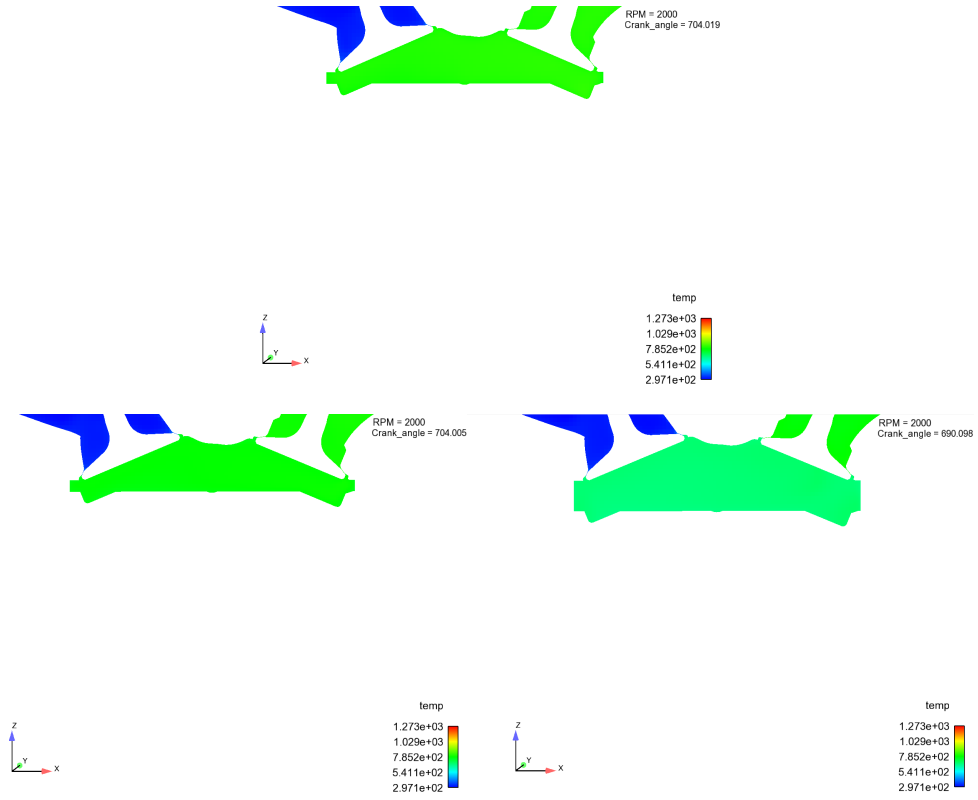


Figure 5.39. Temperature at 5 degCA before spark - 2000x30

At spark advance:

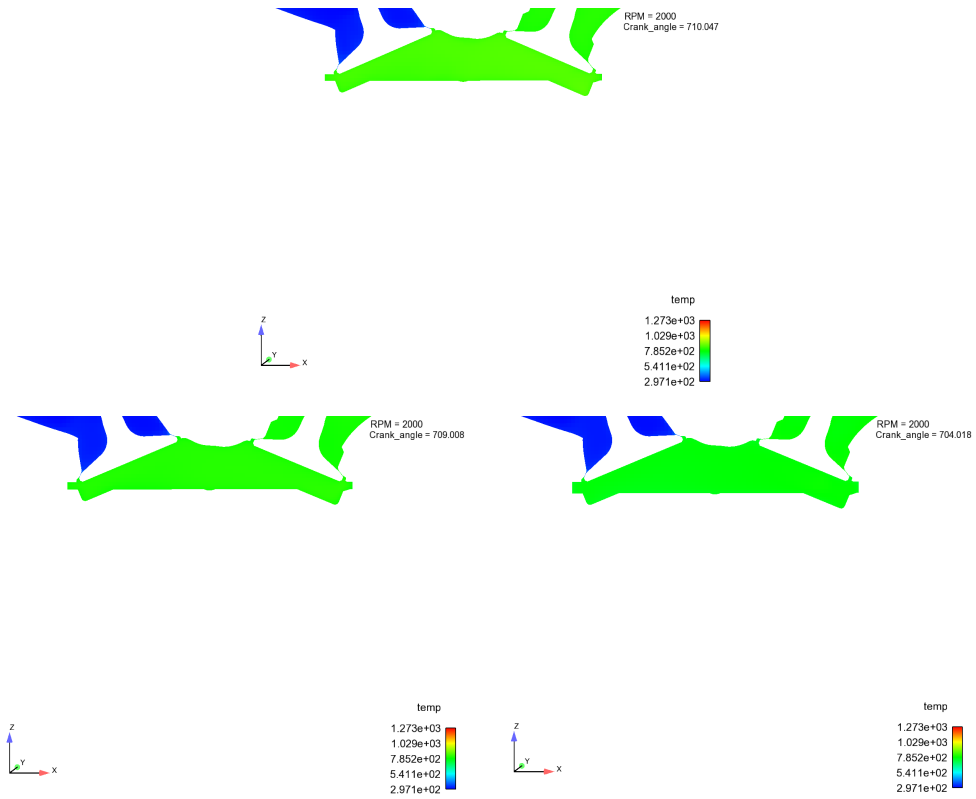


Figure 5.40. Temperature at spark advance - 2000x30

About 5 degCA after spark:

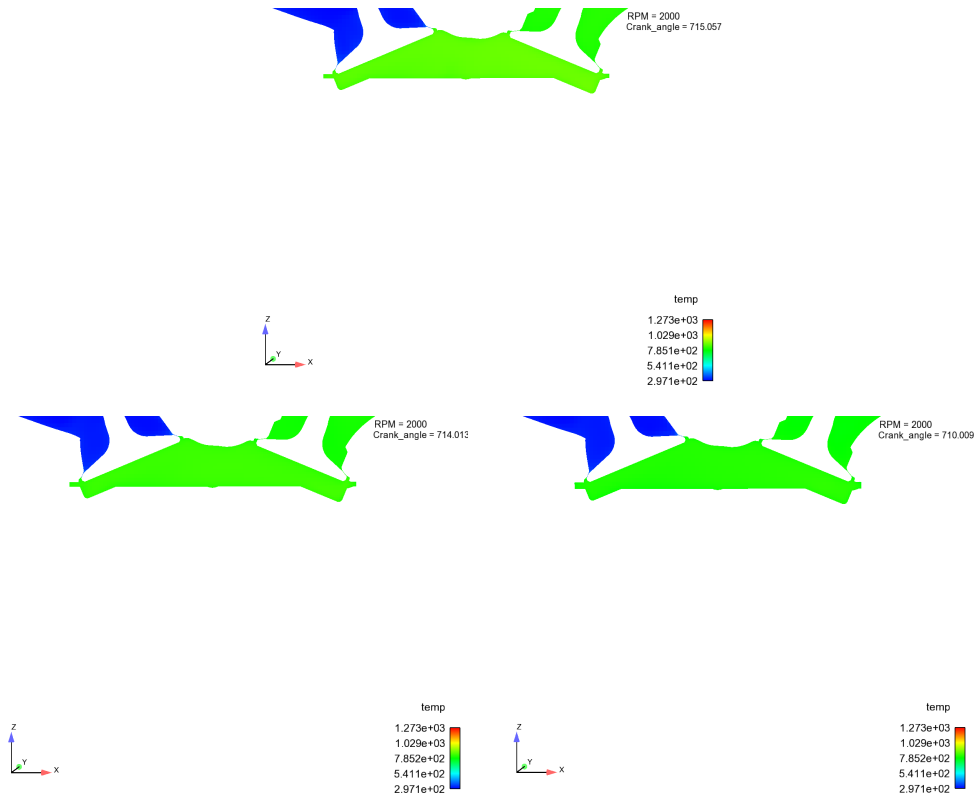


Figure 5.41. Temperature at 5 degCA after spark - 2000x30

At 885 degCA:

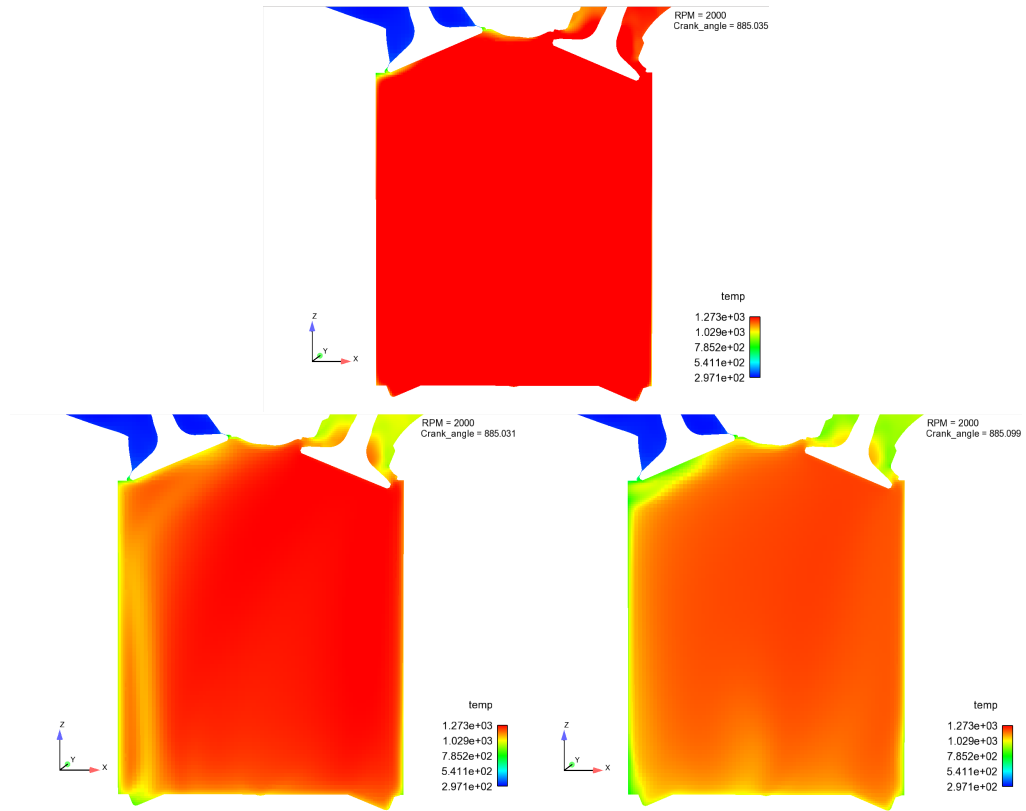


Figure 5.42. Temperature at 885 degCA - 2000x30

At 900 degCA:

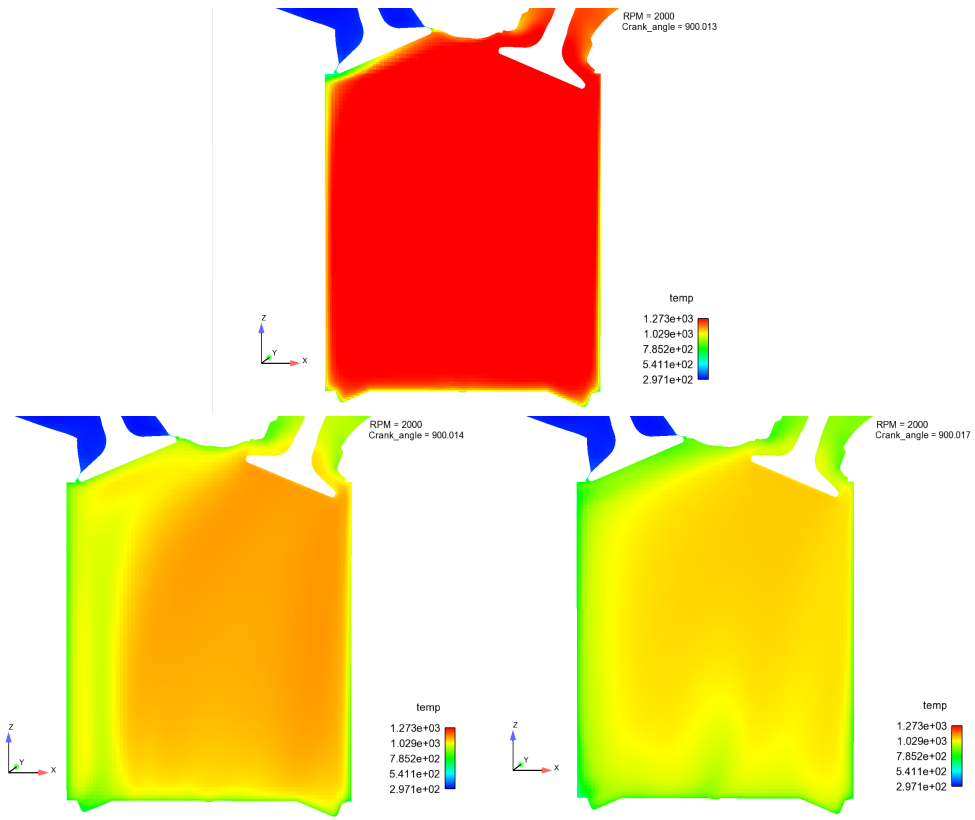


Figure 5.43. Temperature at 900 degCA - 2000x30

At 930 degCA:

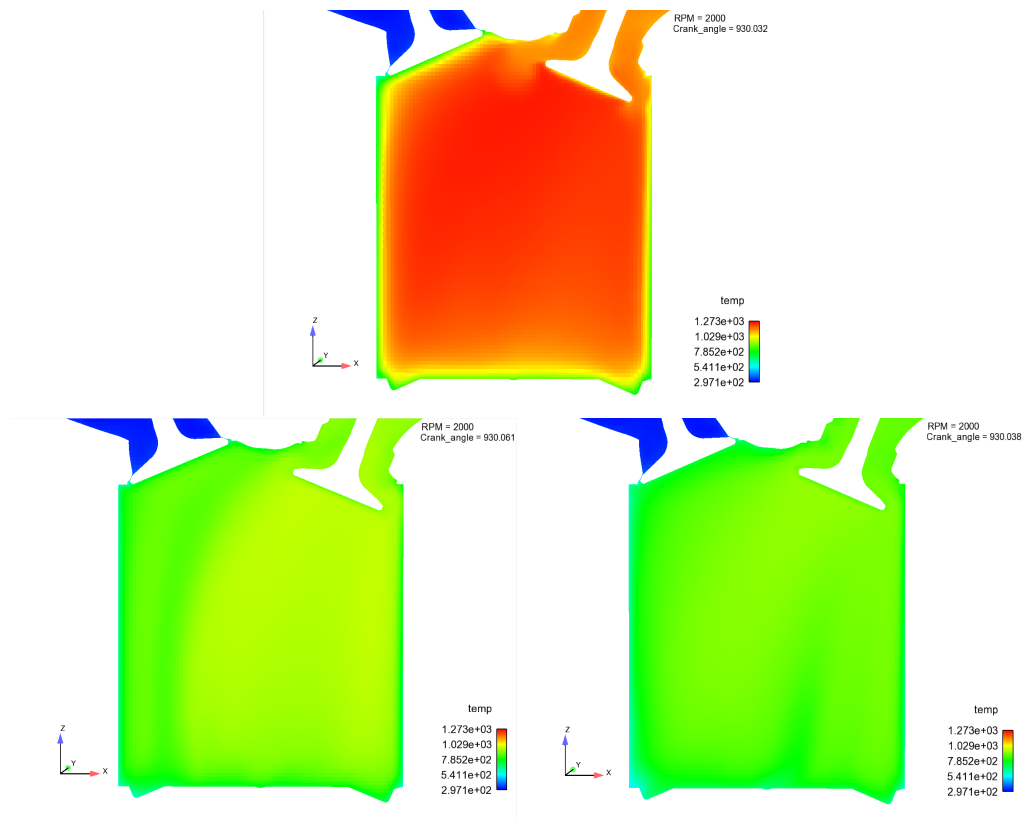


Figure 5.44. Temperature at 930 degCA - 2000x30

At 960 degCA:

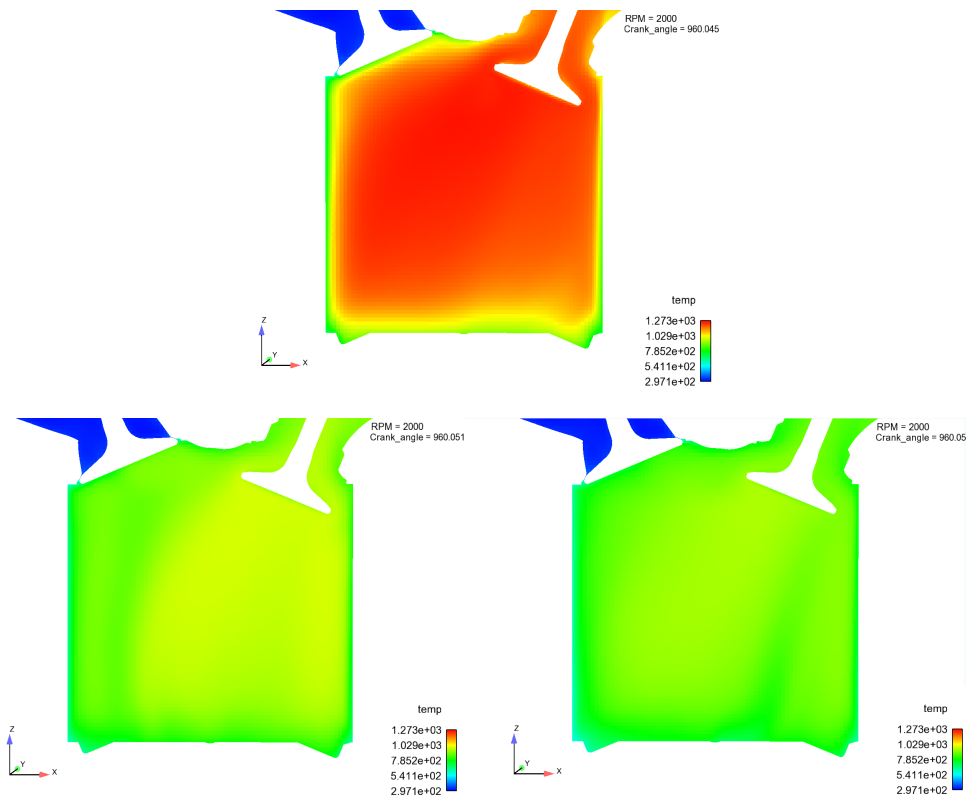


Figure 5.45. Temperature at 960 degCA - 2000x30

5.2.3 Tumble

Tumble is an in-cylinder motion induced by valve. It is a vortex about an axis that is perpendicular to the cylinder one, and it is mainly used in SI engines in order to enhance turbulence. It is generated during expansion and amplified during the first part of compression. Then it is destroyed near TDC and converted into turbulent energy. Plotting the velocity arrows on a plane allows you to see in vortex in the cylinder in the two different phases. Moreover, the comparison at the same crank angle with respect to the spark is made for 2000x8 case.

About 180 degCA before spark:

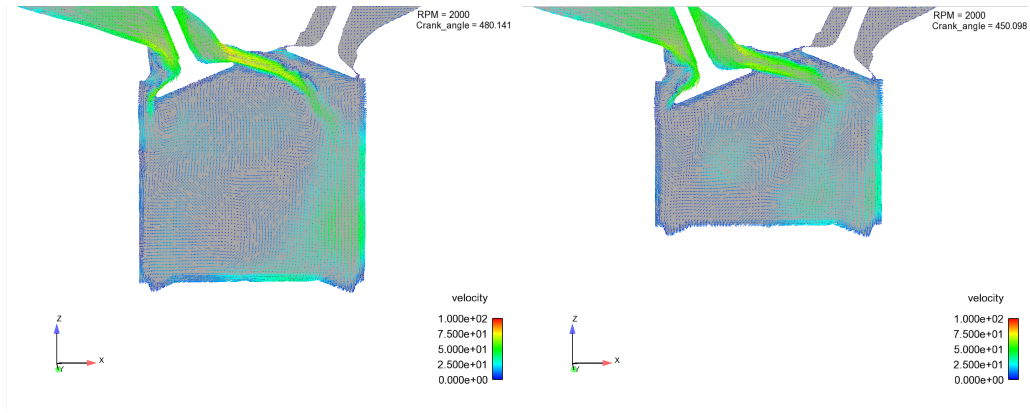


Figure 5.46. Tumble at 180 degCA before spark

About 150 degCA before spark:

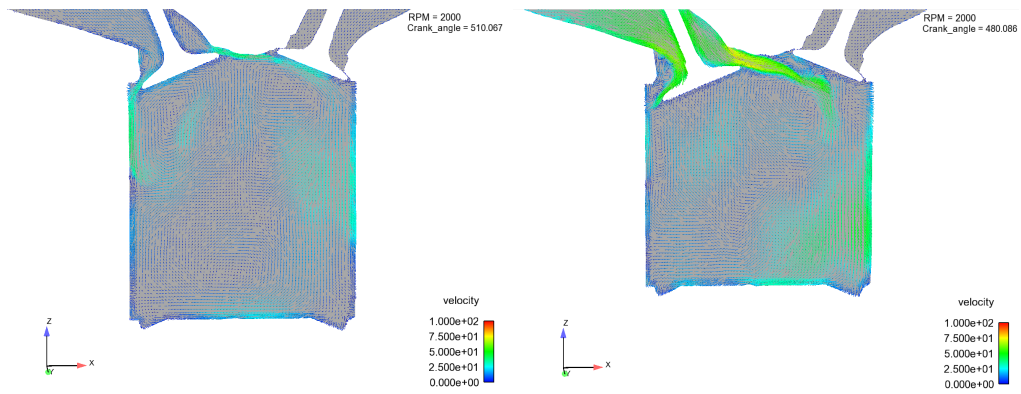


Figure 5.47. Tumble at 150 degCA before spark

About 80 degCA before spark:

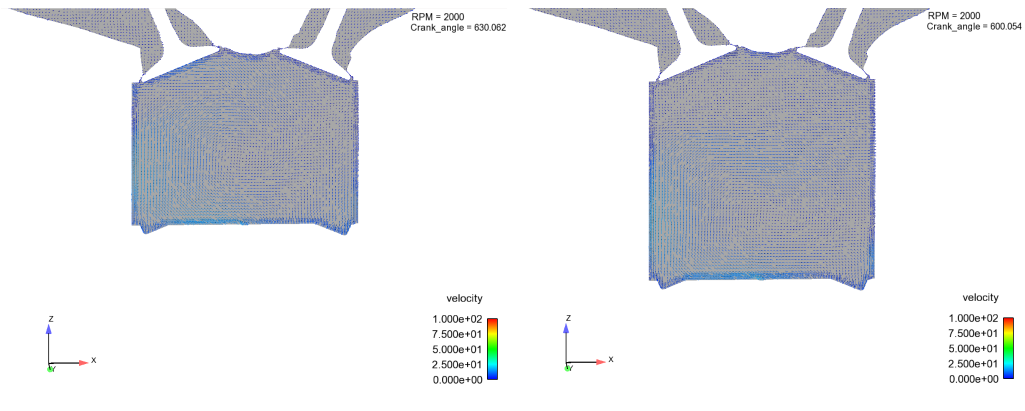


Figure 5.48. Tumble at 80 degCA before spark

About 50 degCA before spark:

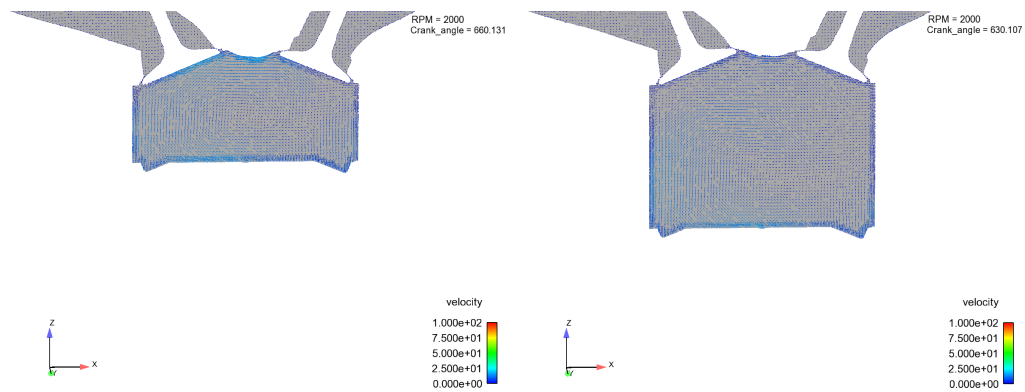


Figure 5.49. Tumble at 50 degCA before spark

About 20 degCA before spark:

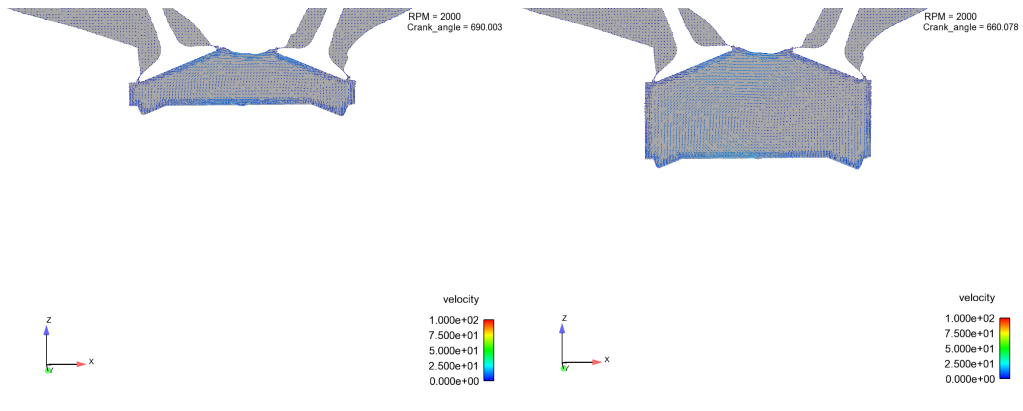


Figure 5.50. Tumble at 20 degCA before spark

At spark advance:

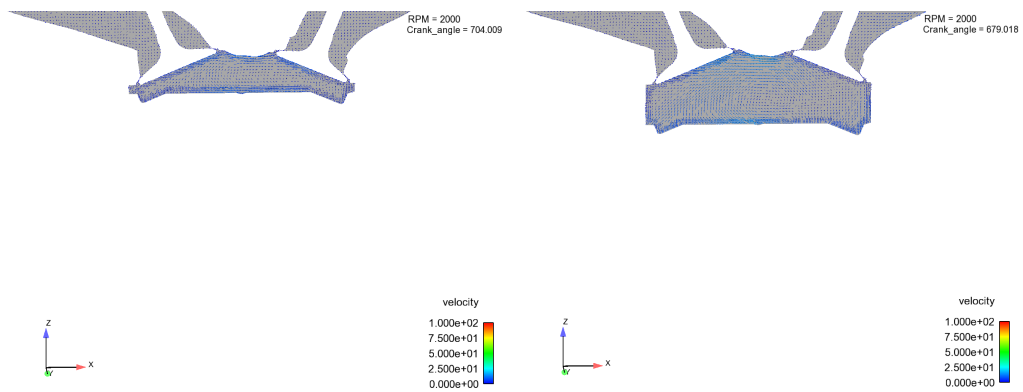


Figure 5.51. Tumble at spark advance

Chapter 6

Conclusion

The document aims at characterize the diluted combustion inside a direct injection engine which works with natural gas. Thanks to its properties, NG results a good alternative to conventional fuel, such as gasoline and diesel, to deal with the new regulations about CO₂ emissions, which set more stringent limits.

Computational fluid dynamics has been used for carrying out the simulations. Equations on which CFD is based and the physical models implemented in the software has been presented and discussed. The 3D-model provided by partners of the project, has been calibrated against experimental data, and the influence of the calibration parameters has been showed. In particular, as α increase, the peak pressure increase and the heat release curve is shifted on the left, meaning that the combustion starts before.

Finally, the model has been used as predictive, in order to investigate working points with no experimental data, and see the influence of EGR on the engine. Starting from test results, an analysis of how engine performance is affected by the mixture dilution has been carried out. The first studies demonstrate that a higher EGR content, leads to a higher coefficient of variation of indicate mean effective pressure. If this value is too hight, combustion become more and more unstable. Also the duration of combustion is affected by recirculating exhaust gas, in fact the

parameter MFB0-50 increases, an exception is the full load case. Also tumble and turbulent intensity have a growing trend, due to the fact that the spark advance increase as the EGR rate increase.

The 3D data analysis, confirms the results mentioned above. In particular plotting the CH₄ fraction, it's easy to see how the NOEGR cases first finish the combustion phase, with respect to the others. It is also interesting to see how temperature changes in the different figures, specially the exhaust one is lower as EGR contents increase, resulting in a higher efficiency. Then, plotting velocity, tumble vortex are presented, and, from the comparison, is clear that as spark advance is higher, the tumble at the spark increase as well.

The model used is a simplified one. In fact in the geometry the injector is absent and an assumption of homogeneous mixture is made. So, as continuation of the work, the model need to be completed, and as a consequence, the set-up of simulations has to be reviewed in order to decrease the computational cost.

Bibliography

- [1] Global Greenhouse Gas Emission Data: www.epa.gov/ghgemissions/global-greenhouse-gas-emissions-data
- [2] Worldwide Emissions Standards: <https://www.delphi.com/sites/default/files/inline-files/delphi-worldwide-emissions-standards-passenger-cars-light-duty-2016-7>
- [3] GasOn website: <http://www.gason.eu>
- [4] T.I. Mohamad, H.H. Geok, "*Comparison of performance, combustion characteristics and emissions of a spark ignition engine fuelled by gasoline and compressed natural gas*"
- [5] T. Korakianitis, A.M. Namasivayam, R.J. Crookes, "*Natural-gas fueled spark-ignition (SI) and compression-ignition (CI) engine performance and emissions*"
- [6] M.U. Aslam, H.H. Masjuki, M.A. Kalam, "*An experimental investigation of CNG as an alternative fuel for a retrofilled gasoline vehicle*"
- [7] Wikipedia, Computational fluid dynamics: https://en.wikipedia.org/wiki/Computational_fluid_dynamics
- [8] Converge CFD Manual (2017)
- [9] John F. Wendt, "*Computational Fluid Dynamics: an Introduction*" Springer, 2009

- [10] J.H. Ferziger, M. Peric, "*Computational Method for Fluid Dynamics*" Springer, 2002
- [11] Norbert Peters, "*Turbulent Combustion*" Cambridge
- [12] O. Colin, A. Benkenida, "*The 3-Zones Extended Coherent Flame Model (ECFM3Z) for Computing Premixed/Diffusion Combustion*", 2004
- [13] O. Colin, K. Truffin, "*A spark ignition model for large eddy simulation based on an FSD transport equation (ISSIM-LES)*", 2011
- [14] J-M Duclos, O. Colin, "*Arc and Kernel Tracking Ignition Model for 3D Spark-Ignition engine calculations*", 2011
- [15] R. Reinman, M. Akram, "*Spark energy deposition studies*", 1998
- [16] R. Scarcellini, T. Wallner, "*A Detailed Analysis of the Cycle-To-Cycle Variations featured by RANS Engine Modeling*"
- [17] T. Poinso, D. Veynante, "*Theoretical and Numerical Combustion*" R.T. Edwards, 2005
- [18] M. Božić, A. Vučetić, "*Experimental investigation on influence of EGR on combustion performance in SI Engine*", 2017
- [19] M. Baratta, D. Misul, E. Spessa, "*Experimental and numerical approaches for the quantification of tumble intensity in high performance SI engine*", 2017
- [20] F. Xie, W. Hong, "*Effect of external hot EGR dilution on combustion, performance and particulate emissions of a GDI engine*", 2017
- [21] M. Zheng, Graham T. Reader, "*Diesel engine exhaust gas recirculation—a review on advanced and novel concepts*", 2003

BIBLIOGRAPHY

- [22] D. Agarwal, S. K. Singh, "*Effect of Exhaust Gas Recirculation (EGR) on performance, emissions, deposits and durability of a constant speed compression ignition engine*", 2010
- [23] Z. Zhang, H. Zhang, "*Effects of tumble combined with EGR (exhaust gas recirculation) on the combustion and emissions in a spark ignition engine at part loads*", 2013
- [24] P.G. Hill, D. Zhang, "*The effects of swirl and tumble on combustion in spark-ignition engines*", 1994
- [25] M. Allenby, W-C. Chang, A. Megaritis, "*Hydrogen enrichment: A way to maintain combustion stability in a natural gas fuelled engine with exhaust gas recirculation, the potential of fuel reforming*", 2001

Vorrei ringraziare i professori Mirko Baratta, Daniela Misul e Ezio Spessa per avermi dato la possibilità di far parte di questo progetto. In questi mesi ho acquisito molte capacità e fiducia, che spero di poter far fruttare al meglio nella mia carriera, e mi ritengo molto fortunata ad averli incontrati durante il mio percorso universitario, sia come insegnanti che come relatori. Inoltre ringrazio tutti i ragazzi che hanno lavorato con me in questo periodo, per essermi stati sempre di supporto e grande aiuto.

Grazie alla mia famiglia, che ha accettato la mia decisione e mi ha permesso di essere qui oggi, nonostante non sia stato facile. Anche se non da vicino, mi è sempre stata accanto condividendo le gioie e gli ostacoli che si sono presentati durante il percorso. Spero di essere sempre all'altezza della fiducia e delle aspettative, soprattutto da ora in avanti.

Grazie ai miei amici lontani, a chi non è potuto esserci e fa comunque il tifo per me, e a chi ha percorso centinaia di km per essere presente. Nonostante tutto, ci sono legami che né il tempo né la distanza cambiano in alcun modo.

Questi anni qui sono volati, ma sono stati profondamente vissuti e hanno rappresentato una grande crescita non solo professionale ma soprattutto personale. Per questo non posso far altro che ringraziare tutte le persone che ho incontrato, che non mi hanno mai fatto sentire sola anche lontana da casa. Grazie per le giornate all'università, le notti di studio, le uscite, le cene, le feste, i pomeriggi al Braccini e i viaggi che abbiamo condiviso. Comunque vadano le cose, rimarrà sempre un bellissimo ricordo di tutto questo.

